Chromosomes and Gene Expression

CyAbrB2 is a nucleoid-associated protein in *Synechocystis* controlling hydrogenase expression during fermentation

Ryo Kariyazono, Takashi Osanai

School of Agriculture, Meiji University

https://en.wikipedia.org/wiki/Open_access

Copyright information

Reviewed Preprint

Published from the original preprint after peer review and assessment by eLife.

About eLife's process

Reviewed preprint version 1
February 8, 2024 (this version)

Sent for peer review
November 22, 2023

Posted to preprint server
November 5, 2023

Abstract

Abstract

The *hox* operon in *Synechocystis* sp. PCC 6803, encoding bidirectional hydrogenase responsible for H2 production, is transcriptionally upregulated under microoxic conditions. Although several regulators for *hox* transcription have been identified, their dynamics and higher-order DNA structure of *hox* region in microoxic conditions remain elusive. We focused on key regulators for the *hox* operon: cyAbrB2, a conserved regulator in cyanobacteria, and SigE, an alternative sigma factor. Chromatin immunoprecipitation-sequencing revealed that cyAbrB2 binds to the *hox* promoter region under aerobic conditions, with its binding being flattened in microoxic conditions. Concurrently, SigE exhibited increased localization to the *hox* promoter under microoxic conditions. Genome-wide analysis revealed that cyAbrB2 binds broadly to AT-rich genome regions and represses gene expression. Moreover, we demonstrated the physical interactions of the *hox* promoter region with its distal genomic loci, and the interactions are lowered in microoxic conditions. In the absence of cyAbrB2, the interactions stayed low both in aerobic and microoxic conditions. From these results, we propose that cyAbrB2 is a cyanobacterial nucleoid- associated protein (NAP), modulating chromosomal conformation, which blocks RNA polymerase from the *hox* promoter in aerobic conditions. We further infer that cyAbrB2, with altered localization pattern upon microoxic conditions, modifies chromosomal conformation in microoxic conditions, which allows SigE-containing RNA polymerase to access the *hox* promoter. The coordinated actions of this NAP and the alternative sigma factor are crucial for the proper *hox* expression in microoxic conditions. Our results highlight the impact of cyanobacterial chromosome conformation and NAPs on transcription, which have been insufficiently investigated.

eLife assessment

The authors provide **solid** data on a functional investigation of potential nucleoid-associated proteins and the modulation of chromosomal conformation in a model cyanobacterium. While the experiments presented are **convincing**, the manuscript could benefit from restructuring towards the precise findings; alternatively, additional data buttressing the claims made would significantly enhance the study. These **valuable** findings will be of interest to the chromosome and microbiology fields.

Introduction

Cyanobacteria carry out oxygenic photosynthesis but sometimes experience microoxic conditions during the night. Subsequently, cyanobacteria perfrom fermentation, using glycolytic products as electron acceptors. (1). Cyanobacteria have multiple fermentation pathways according to the environment. For example, the freshwater living cyanobacterium *Synechocystis* sp. PCC 6803 (hereafter referred to as *Synechocystis*) produces acetate, lactate, dicarboxylic acids, and hydrogen (1, 2). Genetic manipulations on *Synechocystis* have demonstrated that modulating the expression of certain enzymes can alter fermentative metabolic flow (3, 4). This provides evidence that transcription regulates the fermentative pathway.

Hydrogen has attracted significant attention among other cyanobacterial bioproducts owing to its potential as a biofuel. Bidirectional hydrogenase is a key enzyme for H2 production from protons (5) and is commonly found in cyanobacteria (6). Cyanobacterial hydrogenase comprises five subunits (HoxEFUHY) containing nickel and Fe-S clusters (7). This enzyme can utilize NADH, reduced ferredoxin, and flavodoxin as substrates (8). Hydrogenase can also use excess electrons from the photosynthetic electron transport chain, but photosystem II-generated oxygen can inhibit its activity (9). Another metal-ion-harboring and O2-sensitive enzyme, pyruvate-ferredoxin oxidoreductase (PFOR), oxidizes pyruvate to produce acetyl- CoA during fermentation. PFOR works coordinatedly with hydrogenase to reduce ferredoxin, which hydrogenase uses as an electron donor (8, 10). Despite their O2 sensitivity, hydrogenase and PFOR work under mixotrophic (i.e., aerobic) conditions (11, 12). Therefore, uncontrolled expression of *hox* operon and *niff* may hamper metabolism under photosynthetic conditions or shorten the supply of inorganic cofactors. Thus, transcriptional regulation in response to the environment is essential for optimal energy cost performance.

Promoter recognition by RNA polymerases is an essential step in transcriptional regulation. Sigma factors, subunits of RNA polymerase, recognize core promoter sequences. Transcription factors can also bind to promoter regions to suppress or promote RNA polymerase transcription. As well as recruitment or blocking of RNA polymerase, some transcriptional factors, known as Nucleoid-associated proteins (NAPs), modulate chromosomal conformation to regulate transcription (13). NAPs are common in bacteria, but cyanobacterial NAPs remain unidentified, and higher order of DNA structure in cyanobacteria is yet to be shown. A recent study suggested that the manipulation of chromosomal supercoiling impacts transcriptional properties in cyanobacteria (14). There is room for consideration of NAPs modulating chromosomal conformation and regulating expression in cyanobacteria.

In *Synechosysits*, the coding genes of HoxEFUHY form a single operon (sll1220–1226), while PFOR is encoded in the *niff* (sll0741) gene. Both *hox* and *niff* operons are highly expressed under microoxic conditions (15). Genetic analysis has revealed that multiple global transcriptional

regulators control *hox* and *nifJ* expression. Sigma factor SigE (Sll1689) promotes the expression of *hox* and *nifJ* operons (16, 17), while transcription factor cyAbrB2 (Sll0822) represses them (18, 19). Positive regulators for the *hox* operon include LexA (Sll1626) and cyAbrB1 (Sll0359) (20–22).

SigE, an alternative sigma factor, controls the expression of genes involved in glycogen catabolism and glycolysis, as well as PFOR/*nifJ* and hydrogenase (16). SigE shares a high amino acid sequence homology with the primary sigma factor SigA, which is responsible for transcribing housekeeping and photosynthetic genes (23). A ChIP-seq study revealed that, while most SigE-binding sites are the same as SigA, SigE exclusively occupies the promoters of glycogen catabolism and glycolysis (24).

CyAbrB2 and its homolog cyAbrB1 are transcription factors highly conserved in cyanobacteria. For example, cyAbrB homologs in *Anabaena* sp. PCC7120 is involved in heterocyst formation (25). CyAbrB2 in *Synechocystis* regulates the expression of several genes involved in carbon metabolism, nitrogen metabolism, and cell division (19, 26, 27). CyAbrB2 binds to the *hox* promoter *in vitro* and represses its expression *in vivo* (18). CyAbrB1, an essential gene, physically interacts with the cyAbrB2 protein (28) and binds the *hox* promotor region *in vitro* to promote its expression (20).

To explore the dynamics of those transcription factors governing the expression of *hox* operon, we conducted a time-course analysis of the transcriptome and ChIP-seq of SigE and cyAbrB2. Our ChIP-seq and transcriptome analysis showed the NAPs-like nature of cyAbrB2, which prompted us to conduct chromosomal conformation capture assay. 3C analysis revealed the physical interaction between the *hox* promoter region and its downstream and upstream genomic region in the aerobic condition, and that the interaction decreased upon entry to the microoxic condition. Furthermore those interactions in the Δ*cyabrB2* mutant were low both in aerobic and microoxic conditions. From those experiments, we propose that cyAbrB2 modulates chromosomal conformation like NAPs, allowing access to the SigE-containing RNA polymerase complex on the *hox* promoter, by which the *hox* operon achieves distinct expression dynamics. Chromosomal conformation of bacteria is a growing area of interest, and the findings of this study have brought insight into the transcriptional regulation of cyanobacteria.

Results

Transcriptomes on entry to dark microoxic conditions

To understand transcriptional regulation under microoxic conditions, we conducted a time-course transcriptome capturing aerobic and microoxic conditions at 1-, 2-, and 4-hours timepoints (**Figure 1A**). Gene set enrichment analysis based on KEGG pathway revealed that many biological pathways, including photosynthesis and respiration (oxidative phosphorylation), were downregulated under microoxic conditions compared to aerobic conditions (**Figure 1B**). Upregulated pathways included butanoate metabolism and two-component systems, but the actual cyanobacterial catabolic pathway differed slightly from that described in the KEGG pathway. Within 1 hour of switching from aerobic to microoxic conditions, the expression levels of 508 genes increased more than 2-fold. Furthermore, genes with increased expression levels were classified into four based on the time-course (**Figure 1C**). Of the 508 genes, 28 were termed “transiently upregulated genes” due to their decreased expression upon the comparison of 1- and 4- hours incubation under microoxic conditions (log2 fold change < −0.5), and 119 were termed “continuously upregulated genes.”, which continuously increased between 1- and 4-hours incubation under microoxic conditions (log2-fold change > 0.5). Other than 508 genes 2-fold upregulated within 1 hour, 28 genes showed more than 4-fold increment within 4 hours but not upregulated within 1 hour. We combined those “Late upregulated genes” with 508 genes and

referred to as “All upregulated genes” in the subsequent analysis (**Figure 1C**). Mapping the classified genes to central carbon metabolism revealed that *nifJ* encoding PFOR and *hox* operon encoding a bidirectional hydrogenase complex were transiently upregulated (**Figure 1D** and **Table 1**). RTqPCR verified the transient expression of *hoxF*, *hoxH,* and *nifJ* (**Figure S1**).

SigE and cyAbrB2 control the expression of transiently upregulated genes

The functional correlation between hydrogenase and PFOR, encoded by the *hox* operon and *nifJ*, suggests that transient upregulation has physiological significance. We focused on transiently upregulated genes and attempted to reveal the regulatory mechanism underlying transient upregulation. While SigE promotes the expression of *hox* and *nifJ*, cyAbrB2 represses them (16, 18, 19). We confirmed that the deletion of *sigE* and *cyabrb2* (Δ*sigE* and Δ*cyabrb2*, respectively) affected the expression of *hoxF*, *hoxH*, and *nifJ* by RT- qPCR (**Figure S1**). Thus, we conducted a time-course transcriptome analysis of Δ*sigE* and Δ*cyabrb2* under aerobic conditions and after 1- and 2-hours cultivation in dark microoxic conditions (**Figures 2A** and S2A).

The transcriptome data confirmed that SigE and cyAbrB2 regulated *hox* operon expression (**Figure 2B**). At each time point, we searched for differentially expressed genes (DEGs) between mutants and wildtype with a more than 2-fold expression change and a false discovery rate (FDR) less than 0.05. We found that deleting *sigE* or *cyabrb2* preferentially affected the expression of transiently upregulated genes, not limited to *hox* and *nifJ* operons (**Figures 2C** and **2D**). Interestingly, *cyabrb2* deletion resulted in the upregulated expression of transient genes under aerobic conditions, in contrast to 1-hour cultivation under microoxic conditions (**Figure 2C**).

Genome-wide analysis of cyAbrB2, cyAbrB1, and SigE via ChIP-seq

To decipher the regulatory mechanism of transiently upregulated genes, we must first comprehend the fundamental features and functions of these transcriptional regulators. Therefore, a genome-wide survey of cyAbrB2 and SigE occupation (**Figures S2** and **S3**) combined with transcriptome data was done. Specifically, we generated a *Synechocystis* strain in which cyAbrB2 was epitope-tagged and performed a ChIP-seq assay under aerobic and microoxic conditions (**Figures S2B** and **S2C**). SigE-tagged strains previously constructed and analyzed elsewhere were also employed (24). The primary sigma factor SigA was also analyzed to determine SigE-specific binding. In addition to cyAbrB2, we tagged and analysed cyAbrB1, which is the interactor of cyAbrB2 and positively regulates the *hox* operon.

CyAbrB2 binds to long tracts of the genomic region and suppresses genes in the binding region

The ChIP-seq data showed that cyAbrB2 bound to long tracts of the genomic region with lower GC content than the whole genome *Synechocystis* (**Figures 3A** and **3B**). Vice versa, regions exhibiting lower GC contents showed a greater binding signal of cyAbrB2 (**Figure 3C**). This correlation was not a systematic bias of next-generation sequencing because the binding signals of SigE, SigA, and control showed no negative correlation to GC contents (**Figure S4A**). The binding regions of cyAbrB2 called by peak-caller covered 15.7% of the entire genome length. 805 of 3614 genes overlapped with cyAbrB2 binding regions, and almost half (399 of 805 genes) were entirely covered by cyAbrB2 binding regions. The cyAbrB2 binding regions included 80 of 125 insertion sequence elements (**Figure 3D**). Comparison with the transcriptome of Δ*cyabrB2* revealed cyAbrB2 tended to suppress the genes overlapping with its binding regions under aerobic conditions (**Figures 3A** and **3E**). A survey of the genomic localization of cyAbrB1 under aerobic conditions revealed that cyAbrB1 and cyAbrB2 shared similar binding patterns (**Figures 3A** and S4C). Due to the essentiality of cyAbrB1, we did not perform transcriptome analysis on a cyAbrB1- disrupted strain.

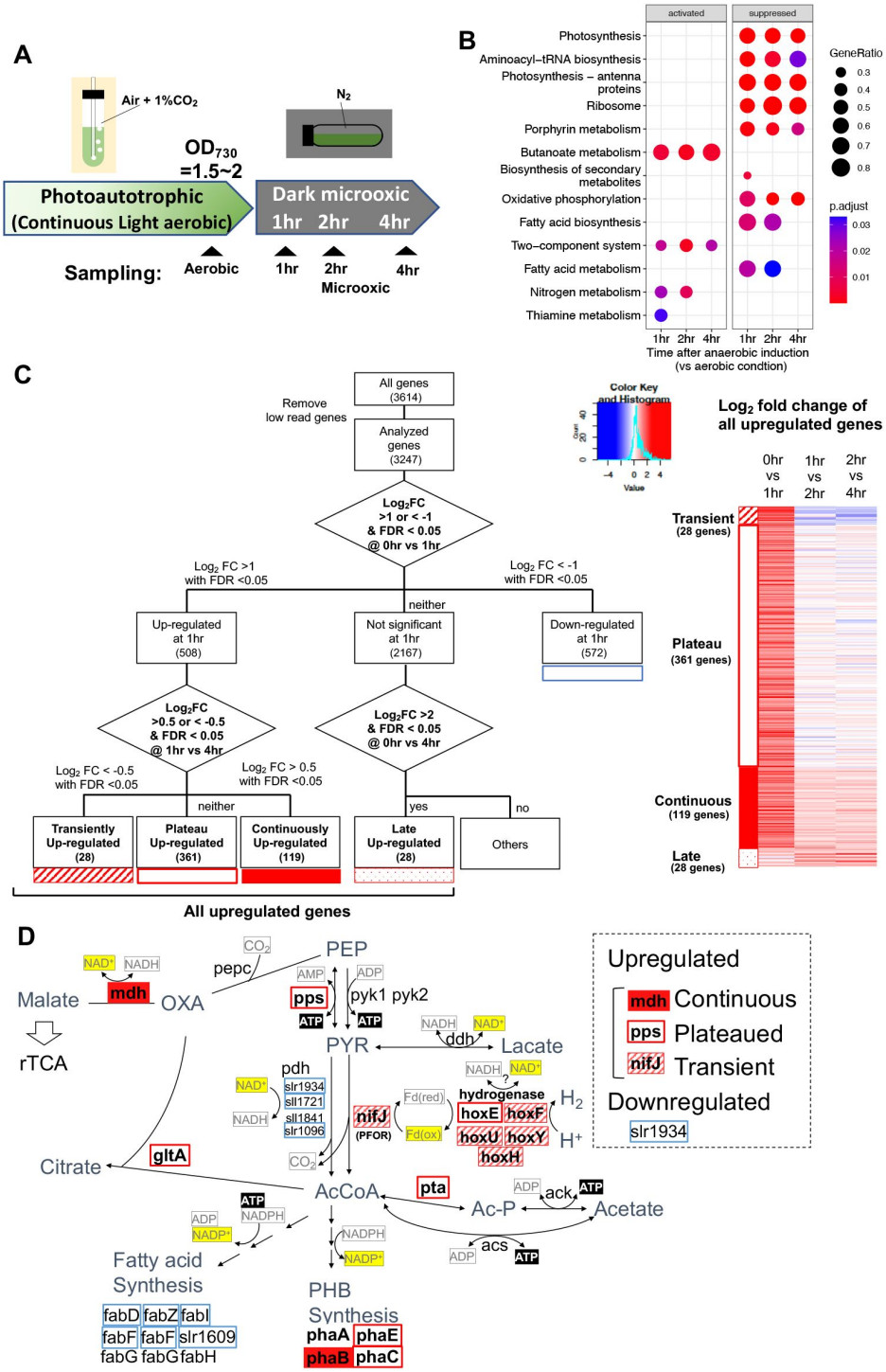

Figure 1

Schematic diagram for the sampling of cells under aerobic and microoxic conditions. (B) Gene set enrichment analysis on time-course transcriptome data. KEGG pathways enriched in upregulated or downregulated genes after 1-, 2-, and 4-h incubation under microoxic conditions are shown. (C) (left) Schematic diagram showing the classification of genes according to the time-course transcriptome. Transient (striped square), Plateau (open square), Continuous (filled square), and Late (dotty square) are denoted as all upregulated genes. (right) Heatmap showing expression change in all upregulated genes over the time-course. Genes were clustered into subgroups and sorted by the gene name. (D) The classified genes were mapped to the central carbon metabolism, centered on pyruvate. PEP: phosphoenolpyruvate, PYR: pyruvate, AcCoA: acetyl CoA, Ac-P: acetyl phosphate, OXA: oxaloacetate, PHB: polyhydroxy butyrate. rTCA: reverse tricarboxylic acid cycle.

		Operon
Oxidoreductase		
sll0741	*nifJ*/"pyruvate-ferredoxin/flavodoxin oxidoreductase"	TU3296
sll0743	hypothetical protein	
sll0744	dihydroorotate dehydrogenase (fumarate)	
sll1221	*hoxF*/“bidirectional [NiFe] hydrogenase diaphorase subunit”	TU1714
sll1222	unknown protein	
sll1223	*hoxU*/“bidirectional [NiFe] hydrogenase diaphorase subunit”	
sll1224	*hoxY*/“NAD-reducing hydrogenase small subunit”	
sll1225	unknown protein	
sll1226	*hoxH*/“NAD-reducing hydrogenase large subunit”	
slr1434	*pntB*/"H+-translocating NAD(P) transhydrogenase subunit beta"	TU1089
Transporter		
sll1450	*nrtA*/“nitrate/nitrite transport system substrate-binding protein”	TU1023
sll1451	*nrtB*/“nitrate/nitrite transport system permease protein”	
sll1452	*nrtC*/“nitrate/nitrite transport system ATP-binding protein”	
sll1453	*nrtD*/“nitrate/nitrite transport system ATP-binding protein”	
Two-component system		
slr1214	twitching motility two-component system response regulator PilG	TU905
slr1215	unknown protein	TU907
Glycosyl transferase		
slr2116	*spsA*/“spore coat polysaccharide biosynthesis protein; SpsA”	TU1673

Table 1

List of transiently upregulated genes

The list of transiently upregulated genes was merged by transcriptional units and sorted by function. The transcriptional unit information was obtained from a previous study (Kopf et al., 2014).

Protease		
sll1009	*frpC*/"iron-regulated protein"	TU491
Insertion sequence (Transposase)		
slr1523	transposase	TU1659
sll1985	transposase	TU1589
sll7001	transposase	NA
sll7003	toxin FitB	TU7001
ssl0172	transposase	TU3163
Other		
slr1260	hypothetical protein	TU1446
slr0668	unknown protein	TU3532
slr5127	unknown protein	TU5127
sll0710	unknown protein	TU97
sll1307	unknown protein	TU1224

Table 1 (continued)

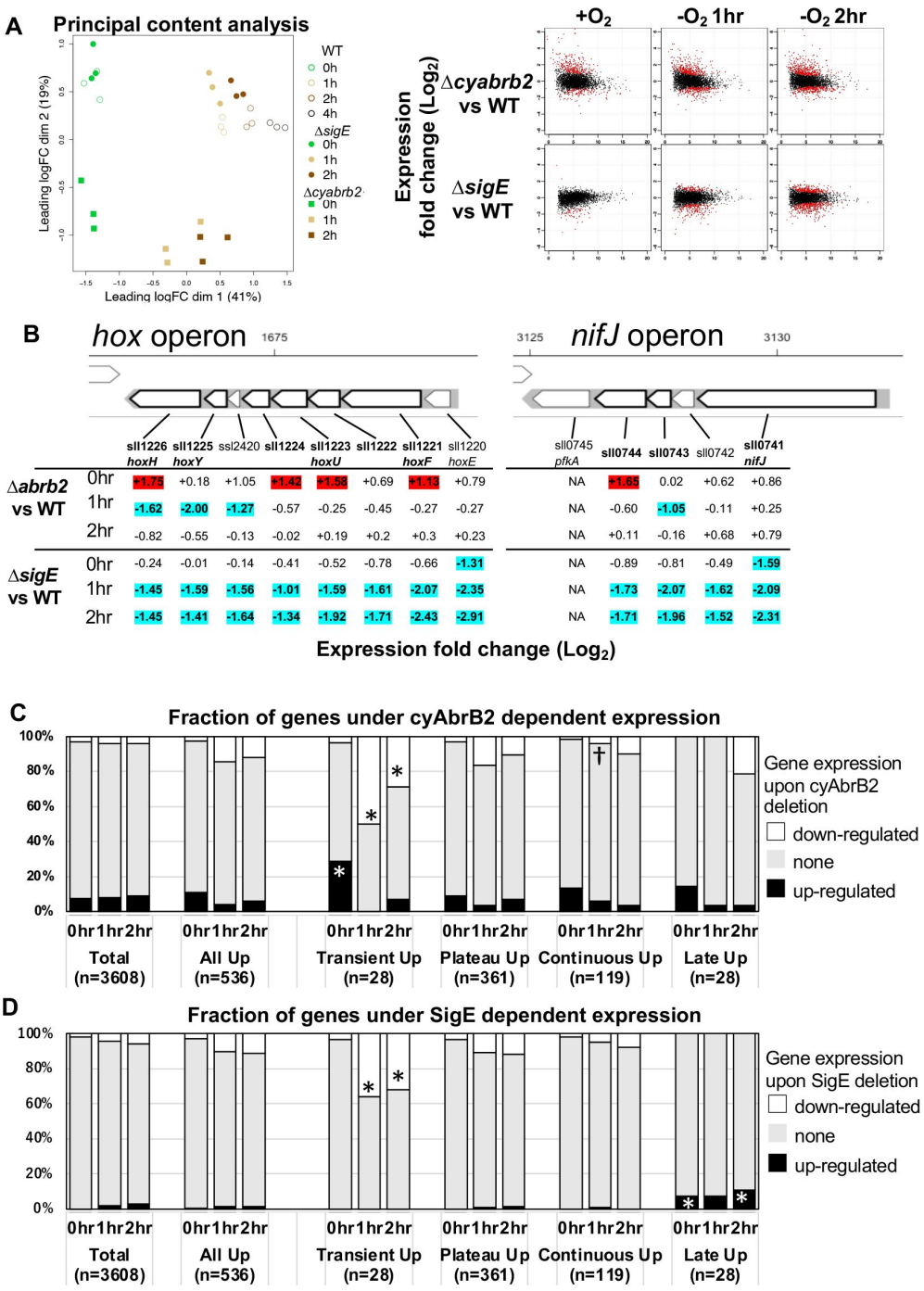

Figure 2

(A) (left) Primary component scatter plot showing the profiles of RNA-seq data. (right) MA plot showing fold change (y-axis) and average (x-axis) of gene expression between wildtype and mutant strains at each timepoint. Red dots indicate defined DEGs (|Log2 FC| >1 with FDR < 0.05). (B) Log2 scaled expression fold change in genes in the *hox* and *nifJ* operons upon Δ*cyabrb2* and Δ*sigE* under aerobic conditions (0, 1 hour after microoxic condition (1 hr), and 2 hours after microoxic condition (2 hr). DEGs are marked with sky blue (downregulated upon deletion) or red (upregulated upon deletion). (C and D) Fraction of upregulated and downregulated genes upon the (C) Δ*cyabrb2* and (D) Δ*sigE* at the timepoints of aerobic conditions (0 hr), 1 hour after anoxic condition (1 hr), and 2 hour after anoxic condition (2 hr). Genes are classified according to **Figure 1C**. Asterisk (*) and dagger (†) denote statistically significant enrichment and anti-enrichment compared with all upregulated genes tested by multiple comparisons of Fisher's exact test (FDR < 0.05).

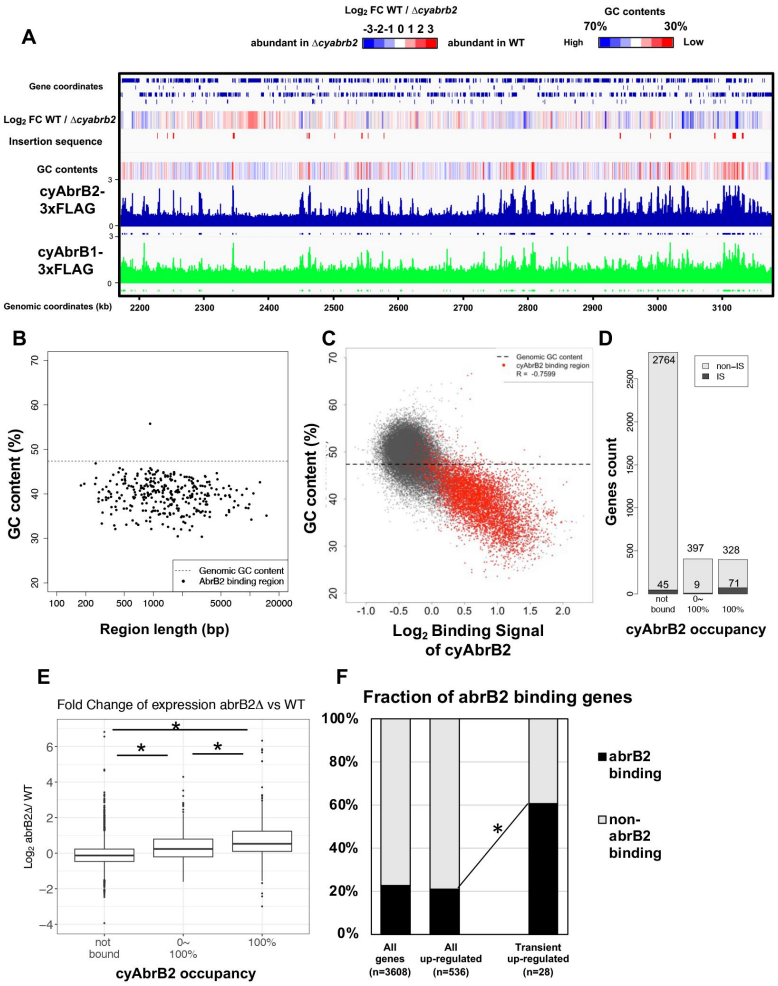

Figure 3

Snapshot of ChIP-seq data for cyAbrB2 and cyAbrB1 under aerobic conditions. The heatmap in the second column indicates expression fold change upon Δ*cyabrb2* under aerobic conditions. Positive values (colored in red) indicate that the gene expression is higher in wildtype than in Δ*cyabrb2*, and negative values (colored in blue) indicate the opposite. The positions for the insertion elements are marked with red in the third column. The heatmap in the fourth column indicates GC contents. High GC content are colored in blue and low GC contents are colored in blue.

(A) GC contents and region length of cyAbrB2 binding regions (black dots). The horizontal dotted line indicates the genomic average of GC content.

(B) Scatter plot of GC content and binding signal of cyAbrB2. The x-axis is the binding signal of cyAbrB2 in each 100 bp region, and the y-axis indicates GC contents within 500 bp windows sliding every 100 base pairs. CyAbrB2 binding regions are marked with red dots.

(C) Histogram of genes showing the extent of occupancy (not bound, partially overlapped, or entirely overlapped) by the cyAbrB2 binding region. The gray bars indicate non-IS genes, and the count numbers of the non-IS genes are displayed on the gray bars. The black bars indicate the IS genes, and the count numbers of the IS genes are displayed above the black bars.

(D) Boxplot showing fold change in gene expression by Δ*cyabrb2* under aerobic conditions. Genes are classified according to the extent of occupancy by the cyAbrB2 binding region. Asterisk (*) denotes statistical significance tested by multiple comparisons of the Wilcoxon-rank test.

(E) Fraction of genes overlapped or non-overlapped with cyAbrB2 binding regions at the timepoints of aerobic conditions. Genes are classified according to **Figure 1C**. Asterisk (*) denotes statistically significant enrichment compared with all upregulated genes tested by multiple comparisons of Fisher's exact test.

(F) Distribution of cyAbrB2 around transiently upregulated genes. ChIP-seq data in aerobic (L + O2) and dark microoxic (D – O2) conditions are overlayed. Arrows with bold lines indicate transiently upregulated genes. Shaded arrows indicate operons whose data were obtained from a previous study. The bars below the graph indicate the binding regions of each protein. The black bar at the top of the figure indicates a length of 10 kbp.

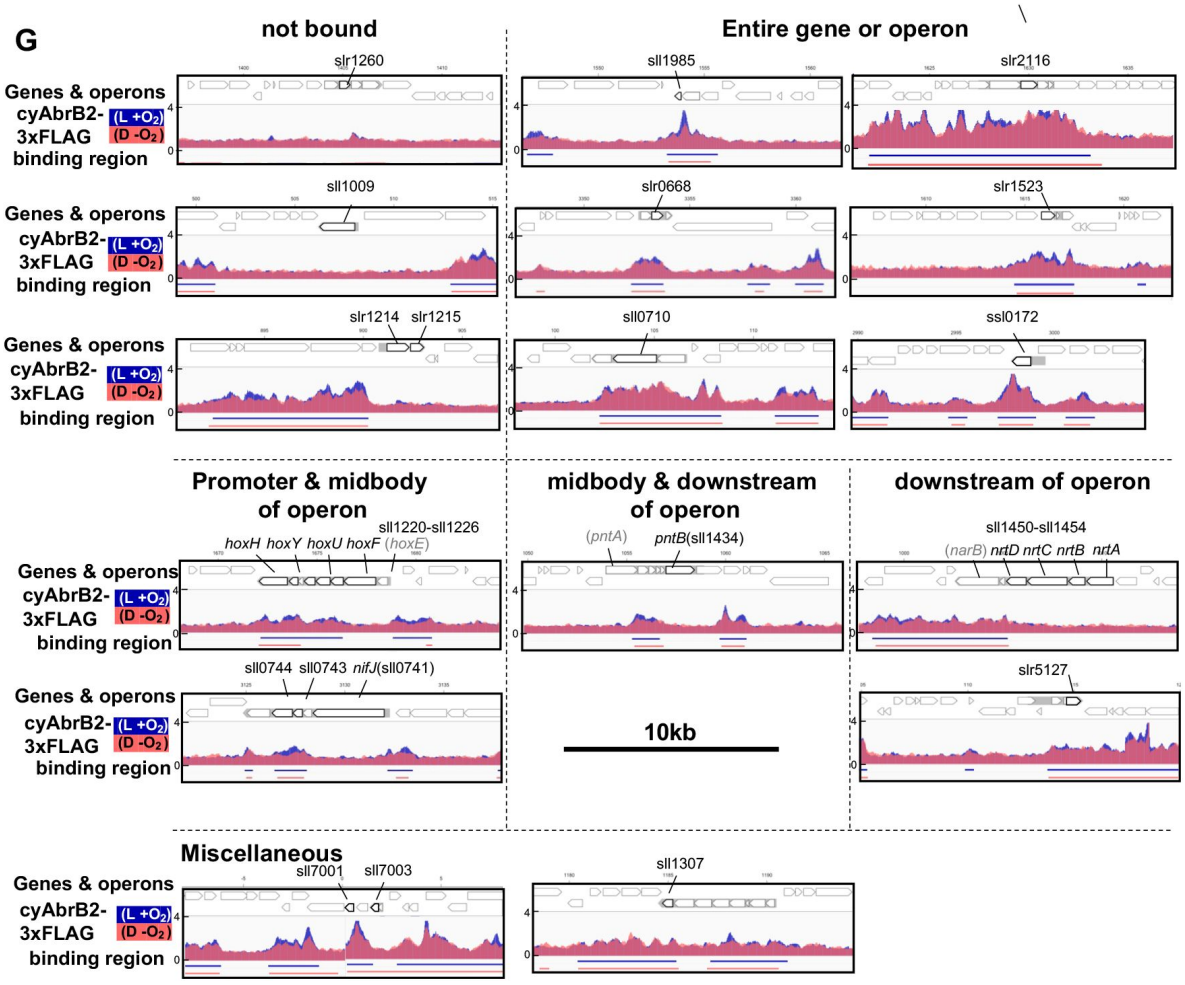

Figure 3 (continued)

Localization of cyAbrB2 became blurry under the microoxic condition

When cells entered microoxic conditions, the relative ChIP-seq signals in the cyAbrB2 binding regions slightly declined (**Figure S5A**). However, the signal change did not necessarily indicate that cyAbrB2 binding declined under microoxic conditions because the relative signal was normalized by total reads of immunoprecipitation and input. Rather, the cyAbrB2 binding pattern became uniform when the cells entered microoxic conditions. Notably, the total quantities of precipitated DNA by tagged cyAbrB2 did not decrease, and qPCR confirmed that the cyAbrB2 binding signal increased in all positions tested (**Figure S5B** and S5C). The protein amount of cyAbrB2 was not altered on entry to the mircooxic condition (**Figure S5D**).

CyAbrB2 binds to transiently upregulated genes

The binding regions of cyAbrB2 overlapped 17 of 28 transiently upregulated genes, showing significant enrichment from all upregulated genes (**Figure 3F**). While cyAbrB2 covered the entire length of insertion sequences and unknown proteins, its binding positions on other transient genes were diverse (**Figure 3G**). Specifically, the *hox* and *nifJ* operons had two distinct binding regions located at the transcription start sites (TSSs) and middle of operons, the *pntAB* operon had two binding regions in the middle and downstream of the operon, and the *nrtABCD* operon had one binding region downstream of the operon (**Figure 3H**). Upon entry into microoxic conditions, the cyAbrB2 binding signal around the transiently upregulated genes became less specific, consistent with the general tendency.

Sigma factors SigE and SigA are excluded from cyAbrB2 binding regions regardless of GC contents

We searched for SigE and SigA binding sites under aerobic and microoxic conditions (**Figures 4A** and **4B**, left and right). The SigE and SigA peaks identified in this study predominantly covered the previously identified peaks (**Figure S2D**), reproducing the previous study's conclusion (24); i.e., SigE and the primary sigma factor SigA share localization on the promoters of housekeeping genes, but SigE exclusively binds to the promoters of its dependent genes. SigE and SigA binding peaks were significantly excluded from the cyAbrB2 binding regions (**Figure 4C**), and signals in cyAbrB2 binding regions were weaker than those in cyAbrB2-free regions (**Figure 4D**). As cyAbrB2 prefers AT-rich regions, we examined whether the peak summits of SigE and SigA were located in regions with high GC contents. Unexpectedly, no correlation was found between the GC content and binding signals of SigE and SigA (**Figures S4A** and **S4B**). Thus, SigA and SigE are excluded from cyAbrB2 binding regions regardless of GC contents.

Dynamics of sigma factors upon exposure to the microoxic condition

When cells entered microoxic conditions, the binding signals of SigA and SigE were changed, although most of their peaks observed under aerobic conditions were present under microoxic conditions (**Figure 4A**). Next, we focused on sigma factor dynamics in transiently upregulated genes. SigE, but not SigA, binds at the TSS of *pntAB* under aerobic and microoxic conditions (**Figure 4E** top). SigE binding summits were not identified at the TSSs of the *hox* and *nifJ* operons under aerobic conditions. However, the SigE-specific binding summit appeared at the TSS of *nifJ* when cells entered microoxic conditions (**Figure 4E** middle). A bimodal peak of SigE was observed at the TSS of the *hox* operon, although the peak caller failed to recognize it as two peaks (**Figure 4E** bottom panel). One side of the bimodal peak marked with an arrow in **Figure 4E** lacked SigA binding. SigE binding without SigA on the promoters of *hox*, *nifJ*, and *pntAB* is consistent with their SigE-dependent expression (**Figure 2B**).

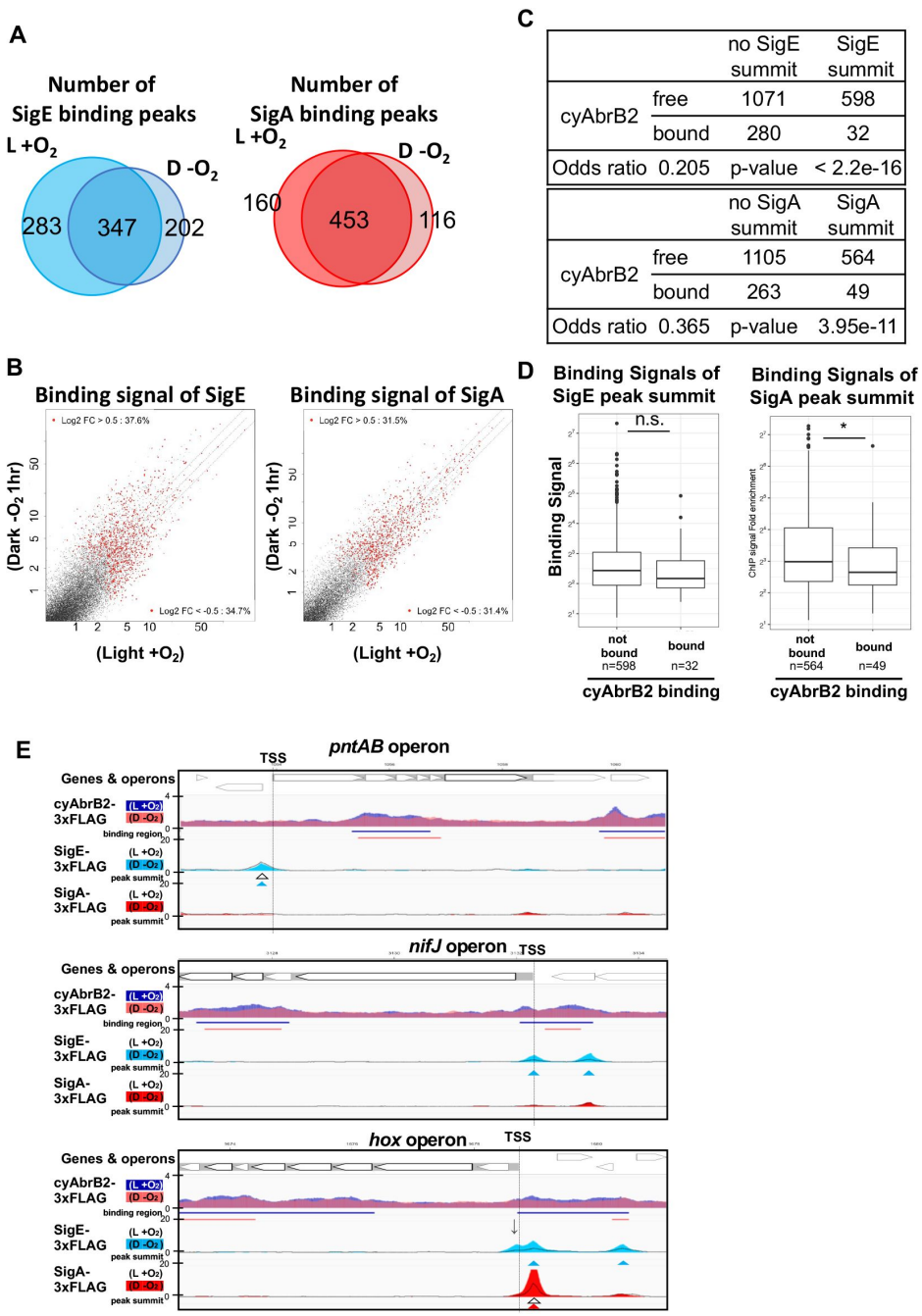

Figure 4

(A) Venn diagram showing the number of peaks of SigE (left) and SigA (right) in aerobic (L + O2) and dark microoxic (D – O2) conditions. (B) Scatter plot showing changes in the binding signal of SigE and SigA by 1 hour cultivation under microoxic conditions. The binding signal of each 100 bp window is plotted. The binding signals are plotted in **Figure 3E**. (C) 2x2 tables showing co-occurrence of cyAbrB2 bindingregions and SigE peaks (top) or SigA binding peaks (bottom). Odds and p-values were calculated by Fisher's exact test. (D) Distribution of ChIP enrichment signals of SigE and SigA peaks. The peaks were classified into two based on whether they overlapped with the cyAbrB2-binding region. (E) Snapshots of ChIP-seq data for CyAabrB2, SigE, and SigA at the *nifJ* region (top) and *hox* region (bottom). ChIP-seq data for cyAbrB2, SigE, and SigA under aerobic and dark microoxic conditions are overlayed. ChIP-seq data of cyAbrB2 under aerobic and microoxic conditions are colored blue and pink, respectively. ChIP-seq data for SigE and SigA are shown in solid lines (aerobic conditions) and filled lines (microoxic conditions). The positions of TSSs were obtained from a previous study (Kopf et al., 2014) and indicated by vertical dotted lines. Open triangles indicate peak summits under aerobic conditions, and solid triangles indicate peak summits under microoxic conditions.

CyAbrB2-dependent and independent chromatin conformation around *hox* operon

We have shown that cyAbrB2 broadly binds to AT-rich genomic regions, including insertion element sequences, and represses expression (**Figures 3B** and **3D**). This is functionally similar to the NAPs (13), which makes us hypothesize that cyAbrB2 modulates chromosomal conformation. Therefore, we conducted the chromatin conformation capture (3C) assay against wildtype and *cyabrb2*Δ strain at aerobic and microoxic conditions (1hr and 4hr). qPCR was performed with unidirectional primer sets, where the genomic fragment containing *hox* operon (hereinafter *hox* fragment) was used as bait (**Figure 5A**). We then observed that the *hox* fragment interacted with its distal downstream (~25 kbp) region and proximal upstream (~10 kbp) region in the aerobic condition (**Figure 5B** and **5C**, locus(c) and (j)). Those interactions were detected both in wildtype and Δ*cyabrb2*. However, the interaction frequency between the *hox* fragment and its distal downstream was higher in wildtype than Δ*cyabrb2* (**Figure S7** locus(c)).

CyabrB2 mediates chromatin conformation changes upon microoxic conditions

When the wildtype cells entered the microoxic condition, the *hox* fragment diminished its interaction with its distal downstream and proximal upstream region (**Figure 5B** locus(c) and (j)). By contrast, the interaction frequency in Δ*cyabrb2* mutant were low and unchanged in the aerobic and microoxic conditions. While the interaction scores exhibit considerable variability, the individual data over time demonstrate declining trends of the wildtype at locus (c) and (j) (**Figure S7**). Furthermore, both wildtype and Δ*cyabrb2* mutant showed increased interaction with the proximal downstream fragments on entry to the microoxic conditions (**Figure 5B** and **5C**, locus (f),(g),(h)). In the wildtype cells, the interaction with locus (g) was transiently elevated at 1 hour of the microoxic condition but decreased to the aerobic level at 4 hours. In summary, 3C analysis demonstrated cyAbrB2-dependent and independent dynamics of chromosomal conformation around the *hox* operon in response to the microoxic condition (**Figure 5D**).

Discussion

Physiological significance of transient upregulation of *hox* and *nifJ* operons

The transcriptional upregulation of fermentative genes in response to the microoxic condition is adaptive for energy acquisition. Our time-course transcriptome showed upregulation of several genes involved in catabolism upon exposure to the microoxic condition. The transient upregulation of *hox* and *nifJ* operons is distinctive among them (**Figure 1D**).

The reason for transient upregulation may be the resource constraints of inorganic cofactors and the reusability of fermentative products. Hydrogenase and PFOR (the product of *nifJ* gene) have iron–sulfur clusters, and hydrogenase requires nickel for its activity (29, 30). Continuous expression of the *hox* operon should be futile under physiological conditions, as the overexpression of *hoxEFUYH* and *hypABDCEF* (hydrogenase maturation factors) does not yield a proportional increase in hydrogenase activity without an adequate nickel supply (31). Furthermore, hydrogenase-produced H2 is diffusive and thus difficult to store and reuse as reducing power when cells return to aerobic conditions. Unlike hydrogen fermentation, the reverse tricarboxylic acid (rTCA) cycle produces dicarboxylic acids, which are reusable for generating NADPH via the TCA cycle under aerobic conditions (32). However, adding bicarbonate to phosphoenolpyruvate (PEP) is a rate-limiting step in the rTCA cycle (33).

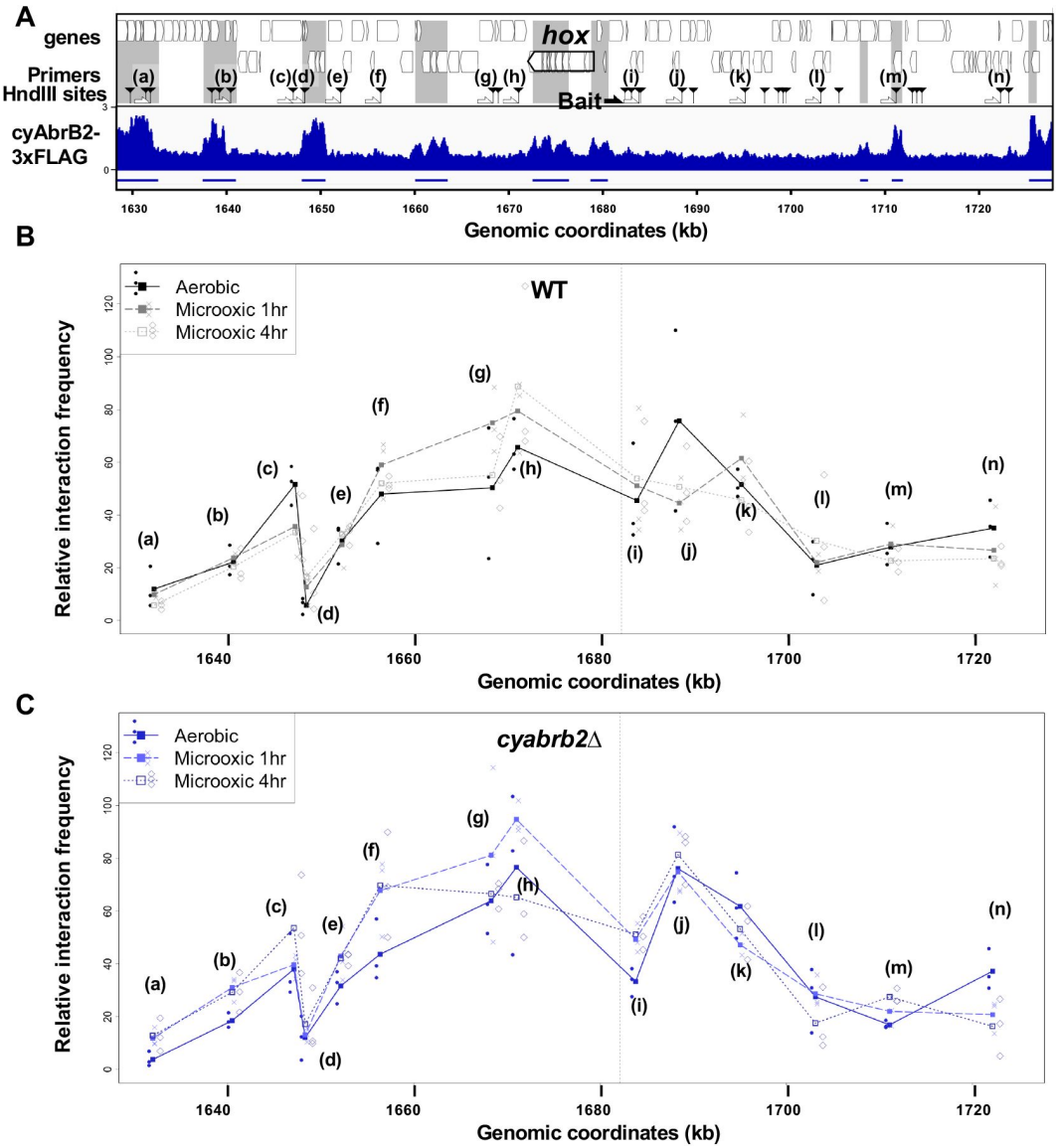

Figure 5

(A) Schematic diagram of 3C analysis around *hox* operon. The black arrow shows the localiton of the bait primer, and white arrows ((a) to (n)) indicate loci where the interaction frequency with bait were assayed. Black arrowheads indicate the position of HindIII sites. ChIP-seq data of cyAbrB2 in the aerobic condition is displayed in the bottom, and cyAbrB2 binding regions are marked with shade. (B) and (C) The line plot showing the interaction frequency of each locus with *hox* fragment in the wildtype (B) and Δ*cyabrb2* (C). The solid, dashed, and dotty lines indicate data in the aerobic condition, 1hr, and 4hr cultivation of microoxic conditions, respectively. The line plots indicate the average interaction frequency over the random ligation (n=3). Indivisual data are plotted as dots. (D) Schematic diagram of the dynamics of transcription factors governing fermentative gene expression. (E) The model showing cyAbrB2 shapes higher order DNA structure of the cyanobacterial chromosome.

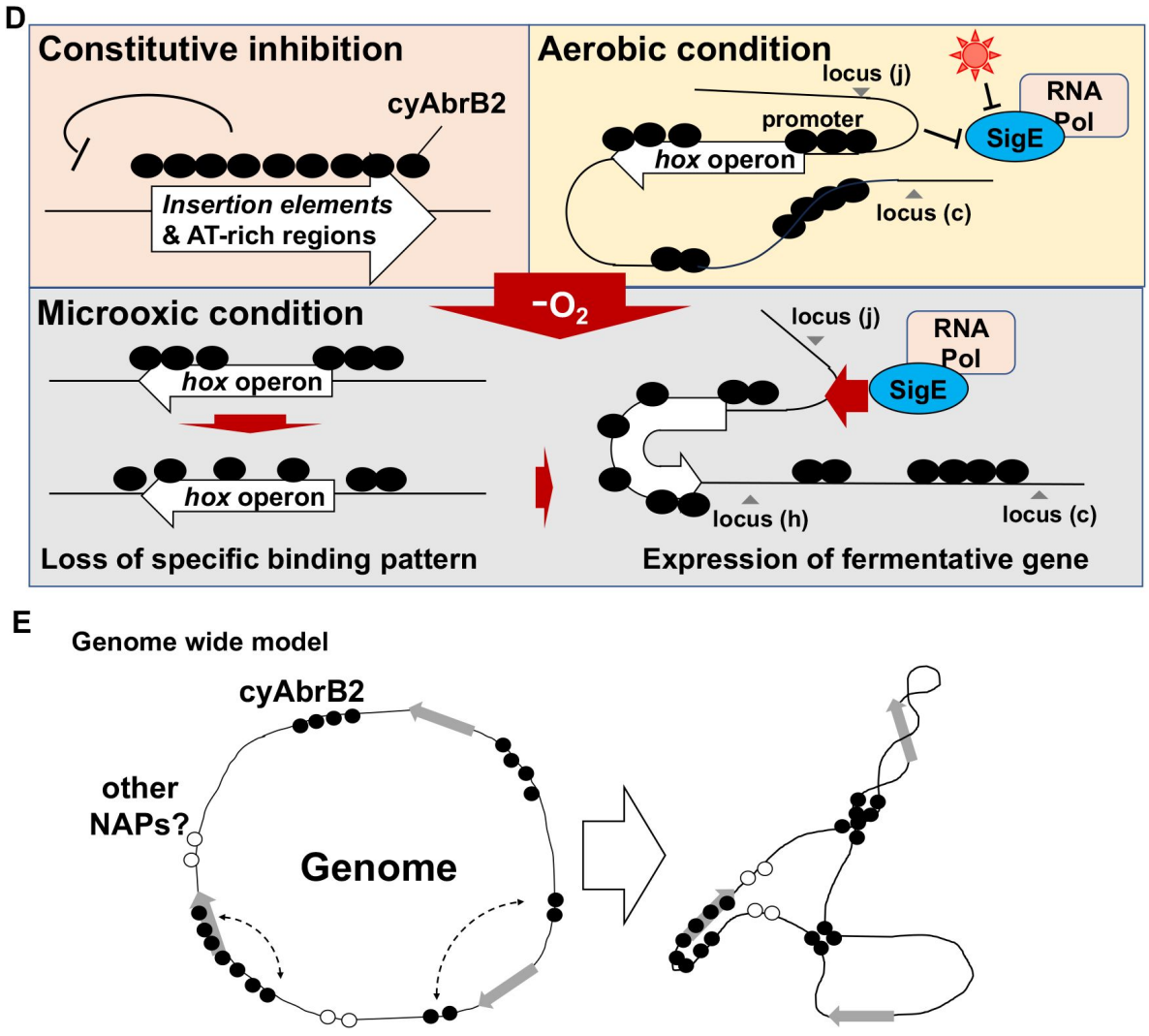

Figure 5 (continued)

Hydrogenase may favor fermentation initiation since it uses only protons as a substrate, and the rTCA cycle may become active subsequently. In fact, *citH*/*mdh* (sll0891) encoding a key enzyme of the rTCA cycle was classified as continuously upregulated genes in this study (**Figure 1D**).

Mechanisms for transient expression mediated by SigE and cyAbrB2

SigE and cyAbrB2 can independently contribute to the transient transcriptional upregulation. This is evident as the single mutants, Δ*sigE* or Δ*cyabrb2*, maintained transient expression of *hoxF* and *nifJ* (**Figure S1**). Here we discuss the cyAbrB2-mediated mechanism, then that of SigE will be discussed.

Three types of the localization pattern and function of cyAbrB2

Herein, we classified three types of binding patterns for cyAbrB2 based on the ChIP-seq data of cyAbrB2. The first is that cyAbrB2 binds a long DNA tract covering the entire gene or operon, represented by the insertion sequence elements. CyAbrB2 suppresses expression in this pattern, as shown in **Figures 3D** and **3E**. In the second pattern, cyAbrB2 binds on promoter regions, such as *hox* operon and *nifJ*. Binding on those promoters fluctuates in response to environmental changes, thus regulating expression. This pattern also applies to the promoter of *sbtA* ($Na^+/HCO3^-$ symporter), as the previous study reported that cyAbrB2 is bound to the *sbtA* promoter in a CO2 concentration-dependent manner (27). The last one is cyAbrB2 binding in the middle or downstream of operons. The middle of *hox*, *pntAB*, and *nifJ* operons and the downstream of *nrt* operon are the cases (**Figure 3G**). Our data show that genes in the same operon separated by the cyAbrB2 binding region behave differently. In particular, *pntB* is classified as the transiently upregulated gene, while *pntA* is not, despite being in the same operon. This might be explained by the recent study which reported that cyAbrB2 affects the stability of mRNA transcribed from its binding gene (34). The cyAbrB2-mediated stability of mRNA may also account for the decrease in transcript from transient upregulated genes at 4 hours of cultivation. Hereafter, we will focus on the mechanism of the second pattern, regulation by cyAbrB2 on the promoter.

Insights into transcriptional regulation of *hox* operon and *nifJ*

Genome-wide analysis indicates that the cyAbrB2-bound region blocks SigE and SigA (**Figures 4C** and **4D**). This is presumably because sigma factors recognize the promoter as a large complex of RNA polymerase. CyAbrB2 binds to the *hox and nifJ* promoter region and may inhibit access to RNA polymerase complex under aerobic conditions. When cells entered microoxic conditions, the binding pattern of cyAbrB2 on the *hox* and *nifJ* promoters got less specific, and SigE binding peaks on those promoters became prominent (**Figure 4E**). Notably, cyAbrB2 ChIP efficiency at the *hox* promoter is higher in the microoxic condition than in the aerobic condition (**Figure S5C**). Hence, the mechanism by which cyAbrB2 inhibits SigE-containing RNAP in the aerobic condition is not solely based on exclusion by occupancy. Rather, it is plausible that chromosomal conformation change governed by cyAbrB2 provides SigE- containing RNAP with access to the promoter region (**Figure 5D**).

Chromosomal conformation in *hox* region changes according to the environmental change

3C analysis demonstrated the interaction between the *hox* promoter and its distal genomic region, which decreased on entry to the microoxic condition. CyAbrB2 mediates the interaction between the *hox* fragment and the distal downstream region. The observed conformational change correlates with the expression of the *hox* operon, though further investigations are needed to establish causality (**Figures 5B** and S7, locus (f), (g), and (j)). A recent study demonstrated that manipulating the expression of topoisomerase, which influence chromosomal conformational change through supercoiling, affect transcriptional properties in cyanobacteria (14). Moreover,

Song et al. pointed out that DNA looping may inhibit transcription in cyanobacteria (34) because artificial DNA looping by the LacI repressor of *E. coli* can repress cyanobacterial transcription (35). Thus, we infer conformation change detected by the present 3C experiment regulates expression of *hox* operon.

A possible mechanism for cyAbrB2-mediated chromosomal conformation

The *hox* promoter region possesses the cyAbrB2 binding region, and locus (c) is adjacent to the cyAbrB2 binding region. Consequently, cyAbrB2 may mediate chromosomal conformation by bridging its binding regions, as other NAPs do. However, no biochemical data mentioned the DNA bridging function of cyAbrB2 in the previous studies (18, 26, 34). CyAbrB1, the homolog of cyAbrB2, may cooperatively work, as cyAbrB1 directly interacts with cyAbrB2 (28), and their distribution is similar (**Figure 3A**). In the microoxic condition, cyAbrB2 binding became blurry, which might reduce the specific interaction between the *hox* region and locus (c). On the other hand, cyAbrB2 indirectly mediates interaction with its proximal upstream region (**Figure 5B**, locus (j)), as this region is devoid of cyAbrB2 binding (**Figure 5A** locus (i) to (l)).

Generality for chromosomal conformation in cyanobacteria

Our 3C analysis revealed that local chromosomal conformation changes upon entry to the microoxic conditions (**Figure 5D**). As cyAbrB2 occupies about 15% of the entire genome and globally regulates gene expression, cyAbrB2 likely governs the whole chromosomal conformation (**Figure 5E**). Furthermore, the conformational changes occur in both AbrB2-dependent and AbrB2-independent manners. Cyanobacteria face various environmental changes besides the microoxic condition, and there are potential NAPs in cyanobacteria yet to be characterized. It is speculated that conformational change of the entire chromosome occurs to deal with many environmental stresses.

The sigE-mediated mechanism for the transient expression

One possible SigE-mediated mechanism for transient expression is the post-transcriptional activation and degradation of SigE in the dark; i.e., SigE is sequestered by binding to the H subunit of Magnesium- chelatase under light conditions and released under dark (36), enabling acute transcription of *hox* operon and *nifJ*. Transcripts of *sigE* were continuously downregulated in our time-course transcriptome, while *sigB* (sll0306) and *sigC* (sll0184) were classified as continuous upregulated genes (**Supplemental Table S1**). It is possible that upregulated SigB and SigC outcompete SigE in prolonged incubation under microoxic conditions. Finally, SigE is degraded under dark within 24 hours (37).

Another reason for the microoxic specific expression may exist in the sequence of the *hox* promoter. We previously determined the consensus sequence of -10 element for SigE regulon in the aerobic condition as “TANNNT,” where N is rich in cytosine (24). The -10 sequence of the *hox* promoter “TAACAA” (22) deviates from the consensus, and no hexamer precisely fitting the consensus are found in the *nifJ* promoter. This deviation can inhibit SigE from binding during aerobic conditions, aside from cyAbrB2-mediated inhibition. Under the microoxic condition, transcription factors LexA (22) and Rre34 (15) may aid SigE binding to the promoter of *hox* and *nifJ*, respectively. Overall, multiple environmental signals are integrated into the *hox* and *nifJ* promoter through the cyAbrB2 and SigE dynamics.

Materials and Methods

Bacterial strains and plasmids

The glucose-tolerant strain of *Synechocystis* sp. PCC 6803 (38) was used as a wildtype strain in this study. The *sigE* (sll1689)-disrupted strain (G50) was constructed in a previous study (16). Disruption and epitope- tagging of *cyabrb1*(sll0359) and *cyabrb2*(sll0822) were performed by homologous double recombination between the genome and PCR fragment (38). The resulting transformants were selected using three passages on BG-11 plates containing 5 μg/mL kanamycin. Genomic PCR was used to confirm the insertion of epitope tag fragments and gene disruption (**Figure S2A**). Supplemental Tables S2, S3, and S4 contain the cyanobacterial strains, oligonucleotides, and plasmids used in this study.

Aerobic and microoxic culture conditions

For aerobic conditions, cells were harvested after 24 hours cultivation in HEPES-buffered BG-110 medium (39), which was buffered with 20 mM HEPES-KOH (pH 7.8) containing 5 mM NH4Cl under continuous exposure to white light (40 μmol $m^{-2}s^{-1}$) and bubbled with air containing 1% CO2 (final OD730 = 1.4–1.8). For the dark microoxic culture, the aerobic culture cell was concentrated to an OD730 of 20 with the centrifuge and resuspended in the culture medium. The concentrated cultures were poured into vials, bubbled with N2 gas, and sealed. The sealed vials were shaded and shaken at 30°C for the described times.

Antibodies and immunoblotting

Sample preparation for immunoblotting was performed as previously described (24), and FLAG-tagged proteins were detected by alkaline-phosphatase-conjugated anti-FLAG IgG (A9469, Sigma Aldrich, St. Louis, MO) and 1-Step NBT/BCIP substrate solution (Thermo Fisher Scientific, Waltham, MA).

RNA isolation

Total RNA was isolated with ISOGEN (Nippon gene, Tokyo, Japan) following the manufacturer's instructions and stored at −80°C until use. The extracted RNA was treated with TURBO DNase (Thermo Fisher Scientific) for 1 hour at 37°C to remove any genomic DNA contamination. We confirmed that the A260/A280 of the extracted RNA was >1.9 by NanoDrop Lite (Thermo Fisher Scientific). We prepared triplicates for each timepoint for the RNA-seq library. RT-qPCR was performed as discribed elsewhere (37).

ChIP assay

Two biological replicates were used for each ChIP-seq experiment, and one untagged control ChIP was performed. ChIP and qPCR analyses were performed using the modified version of a previous method (24). FLAG-tagged proteins were immunoprecipitated with FLAG-M2 antibody (F1804 Sigma-Aldrich) conjugated to protein G dynabeads (Thermo Fisher Scientific).

Library preparation and next-generation sequencing

For the ChIP-seq library, input and immunoprecipitated DNA were prepared into multiplexed libraries using NEBNext Ultra II DNA Library Prep Kit for Illumina (New England Biolabs, Ipswich, MA). For the RNA-seq library, isolated RNA samples were deprived of ribosomal RNA with Illumina Ribo-Zero Plus rRNA Depletion Kit (Illumina, San Diego, CA) and processed into a cDNA library for Illumina with the NEBNext Ultra II Directional RNA Library Prep Kit for Illumina (New England Biolabs). Dual-index primers were conjugated with NEBNext Multiplex Oligos for Illumina (Set1, New England Biolabs). We pooled all libraries, and the multiplexed libraries were dispatched to Macrogen Japan Inc. and subjected to paired-end sequencing with HiSeqX. Adapter trimming and

quality filtering of raw sequence reads were conducted with fastp (ver. 0.21.0) (40) under default conditions. The paired-end sequences were mapped onto the *Synechocystis* genome (ASM972v1) using Bowtie2 (41) (ver. 2.4.5 paired-end). Supplementary Table S5 contains the read counts that passed via fastp quality control and were mapped by Bowtie2.

RNA-seq analysis

Mapped reads were counted by HT-seq count (ver. 2.0.2) (42) for the GFF file of ASM972v1, with the reverse-strandedness option. EdgeR package (ver. 3.40.1) (43) was used to perform the differential expression analysis. Fold changes in expression and FDR were used for gene classification. Supplemental Table S6-S8 contains fold change in gene expression calculated by edgeR.

Genome-wide analyses

Peaks were called using the MACS3 program (ver. 3.0.0b1) (44). For paired-end reads for SigE, SigA, and untagged control ChIP, narrow peaks were called with <1e−20 of the q-value cut-off and "--call- summits" options. The peak summits from two replicates and the untagged control were merged if summits were located within 40 bp of each other. Peak summits identified in both replicates but not in the control, were considered for further analysis. The midpoint of the peak summits for the two merged replicates was further analyzed.

Broad peak calling methods were applied to paired-end reads for cyAbrB2, cyAbrB1, and untagged control ChIP using the "–broad" option, with a q-value cut-off of < 0.05 and a q-value broad cut-off of < 0.05. The intersection of broad peaks from two replicates, excluding those called by the control, was used in subsequent analyses.

The positions of the TSS, including internal start sites, were obtained as reported by (45). The read count, merging, and the intersection of the binding region were calculated using BEDTools (ver. 2.30.0) (46). Supplemental Tables S9–S15 contain SigA and SigE peaks and the broad binding regions of cyAbrB2 and cyAbrB1, respectively.

Binding signals in every 100 bp bin for scatter plots were calculated as (IP read counts within 100 bp window) / (input read counts within 100 bp window) * (total input read counts/total IP read counts). GC contents were calculated within 500 bp in 100 bp sliding windows by seqkit (ver. 2.3.0) (47).

Genome extraction, digestion, and ligation for 3C assay

A 3C assay was conducted based on the previous prokaryotic Hi-C experiment (48, 49), with certain steps modified. To begin, *Synechocystis* were fixed with 2.5% formaldehyde for 15 minutes at room temperature. Fixation was terminated by adding a final concentration of 0.5M of glycine, and cells were stored at -80°C until use. Fixed cells were disrupted using glass beads and shake master NEO (Bio Medical Science, Tokyo, Japan), following the previous study's instructions for preparing cell lysate for ChIP. The lysates were incubated with buffer containing 1mM Tris-HCl (pH7.5), 0.1mM EDTA, and 0.5% SDS for 10min at room temperature, and 1% Triton X-100 quenched SDS. Genomes in the cell lysate were digested by 600U/mL of HindIII (Takara Bio, Shiga, Japan) for 4 hours at 37°C, and RNA in the lysate was simultaneously removed by 50 μg/mL of RNaseA (Nippon genetics, Tokyo, Japan). The digestion was terminated by adding 1% SDS and 22 mM EDTA. The fill-in reaction and biotin labeling steps were omitted from the procedure. The digested genomes were diluted by ligation buffer containing 1% triton-X100 to the final concentration of approximately 1μg/mL and incubated for 10 min at room temperature. Ligation was performed with 2 U/mL of T4 DNA ligase (Nippon Gene) overnight at 16°C. Crosslinking was

reversed under 65°C for 4 hours in the presence of 2.5 mg/mL of proteinase K (Kanto Chemical, Tokyo, Japan), and DNA was purified with the phenol-chloroform method and ethanol precipitation method.

Preparation of calibration samples for 3C qPCR

Based on a previous study, calibration samples for possible ligated pairs were prepared in parallel with 3C ligation (50). In brief, the purified genome of *Synechocystis* was digested by HindIII, and DNA was purified with the phenol-chloroform and ethanol precipitation. Purified DNA was dissolved into the ligation buffer at a concentration of about 600ng/μL and ligated with 2 U/mL of T4 DNA ligase at 16°C overnight. As a result, DNA ~600-fold condensed DNA than 3C samples were ligated.

Quantification of crosslinking frequency for 3C assay

Before the real-time PCR assay, we confirmed that each primer set amplified single bands in a ligation- dependent manner by GoTaq Hot Start Green Master Mix (Promega, Madison, WI) (**Figure S6**). Real-time PCR was performed with StepOnePlus (Applied Biosystems, Foster City, CA) and Fast SYBR Green Master Mix (Thermo Fisher Scientific) according to the manufacturer's instructions. Interaction frequency was calculated by ΔΔCt method using dilution series of calibration samples described above. We confirmed each primer set amplified DNA fragment with a unique Tm value. The amount of the bait fragment containing *hox* operon were quantified and used as an internal control. Supplemental Table S4 contains the list of primers used in the 3C quantification. Interaction frequency for each primer position was calculated as the relative abundance of ligated fragments against the calibration samples and normalized among samples by internal control.

Statistical analysis

Statistical analyses were performed with R version 4.2.2 (51). The "fisher.test" function was used for Fisher's exact test, and p-values < 0.05 were denoted as asterisks in the figure. Multiple comparisons of Fisher's exact test were conducted using "fisher. Multcomp" function in the RVAideMemoire package (52), where p-values were adjusted by the "fdr" method and FDRs <0.05 are shown in the figures. Multiple comparisons of the Wilcoxon-rank test were conducted by "pairwise.wilcox.test," and p-values were adjusted by the "fdr" method. Adjusted p-values < 0.05 are shown in the figure. The correlation coefficient was calculated with the "cor" function. Gene set enrichment analysis (GSEA) was performed by culsterPlofiler package (53) in R with p-value cut-off of 0.05. The enriched pathways detected by GSEA are listed in Supplemental Table S16.

Manuscript writing

We employed GPT-3.5 to refine the expression of the manuscripts.

Accession Numbers

Raw ChIP sequencing and RNA sequencing reads were deposited in the Sequence Read Archive (accession ID: PRJNA956842).

Declaration of interest

The authors declare no competing interests.

Acknowledgements

This study was supported by the following grants to T.O.: Grant-in-Aid for Scientific Research (B) (grant no. 20H02905), JST-ALCA of the Japan Science and Technology Agency (grant number JPMJAL1306), and the Asahi Glass Foundation. We thank Dr. Kohki Yoshimoto for providing laboratory instruments and Ms. Kaori Iwazumi for the support of bacterial culture and the medium preparation.

Author contributions

R.K. and T.O. designed the study; R.K. conducted the experiment; R.K. analyzed the data; R.K. and T.O. wrote the paper.

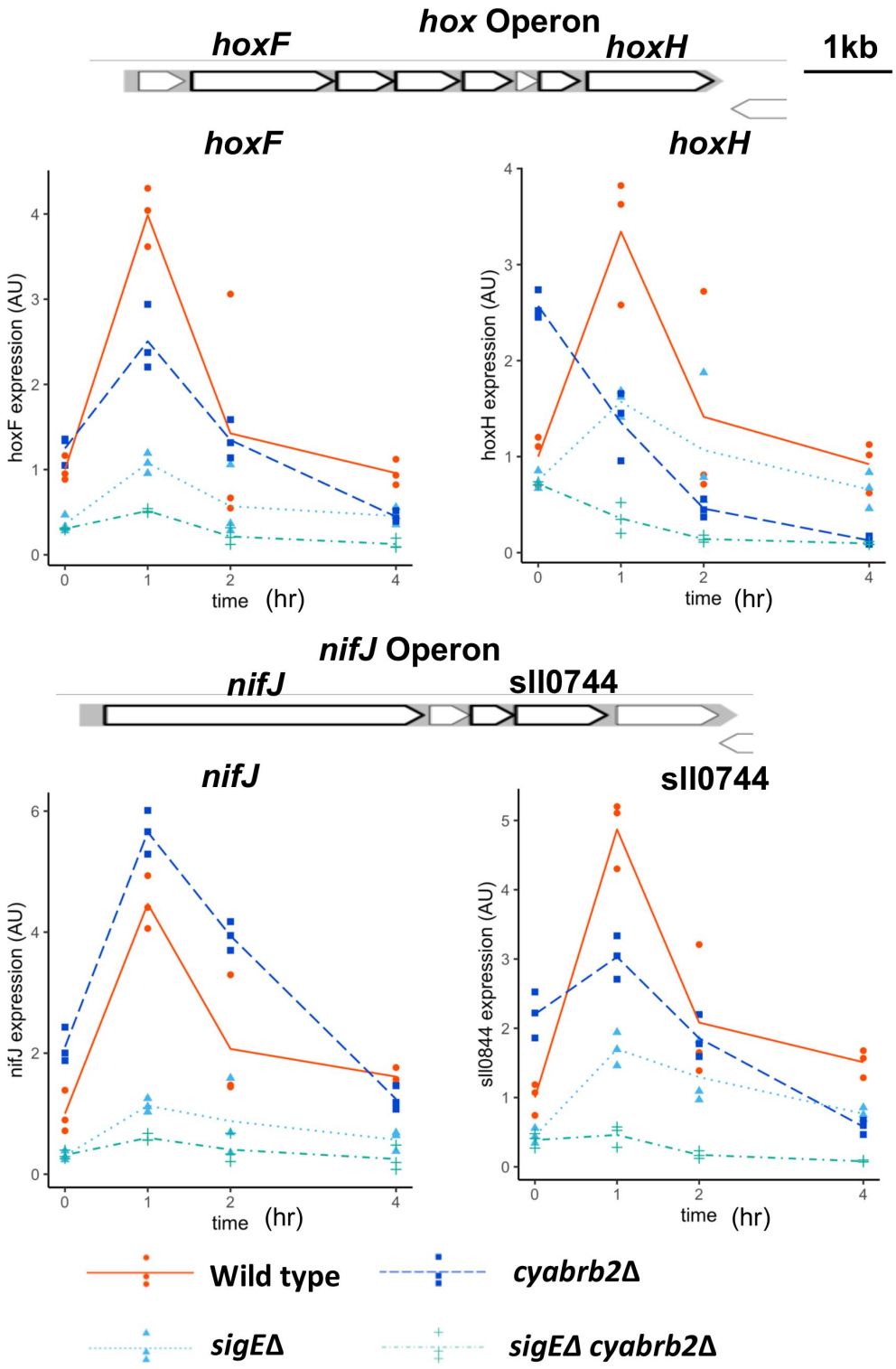

Figure S1

RT-qPCR validated the transiently upregulated genes classified by RNAseq. Transcripts extracted from wildtype (solid line), Δ*sigE* mutant (dotty line), Δ*cyabrb2* mutant (dashed line), and Δ*sigE* Δ*cyabrb2* double mutant (dot-dashed line) were assayed in the aerobic condition (0hr) and 1,2,4 hour incubation of microoxic conditions. As the representative of the transiently upregulated genes, expression of *hoxF*, *hoxY*, *nifJ*, and *sll0744* were quantified by RT-qPCR. The line represents the mean of n=3, and individual data points are shown as dot plots. Data of each gene is normalized by the mean score of wildtypes in the aerobic condition.

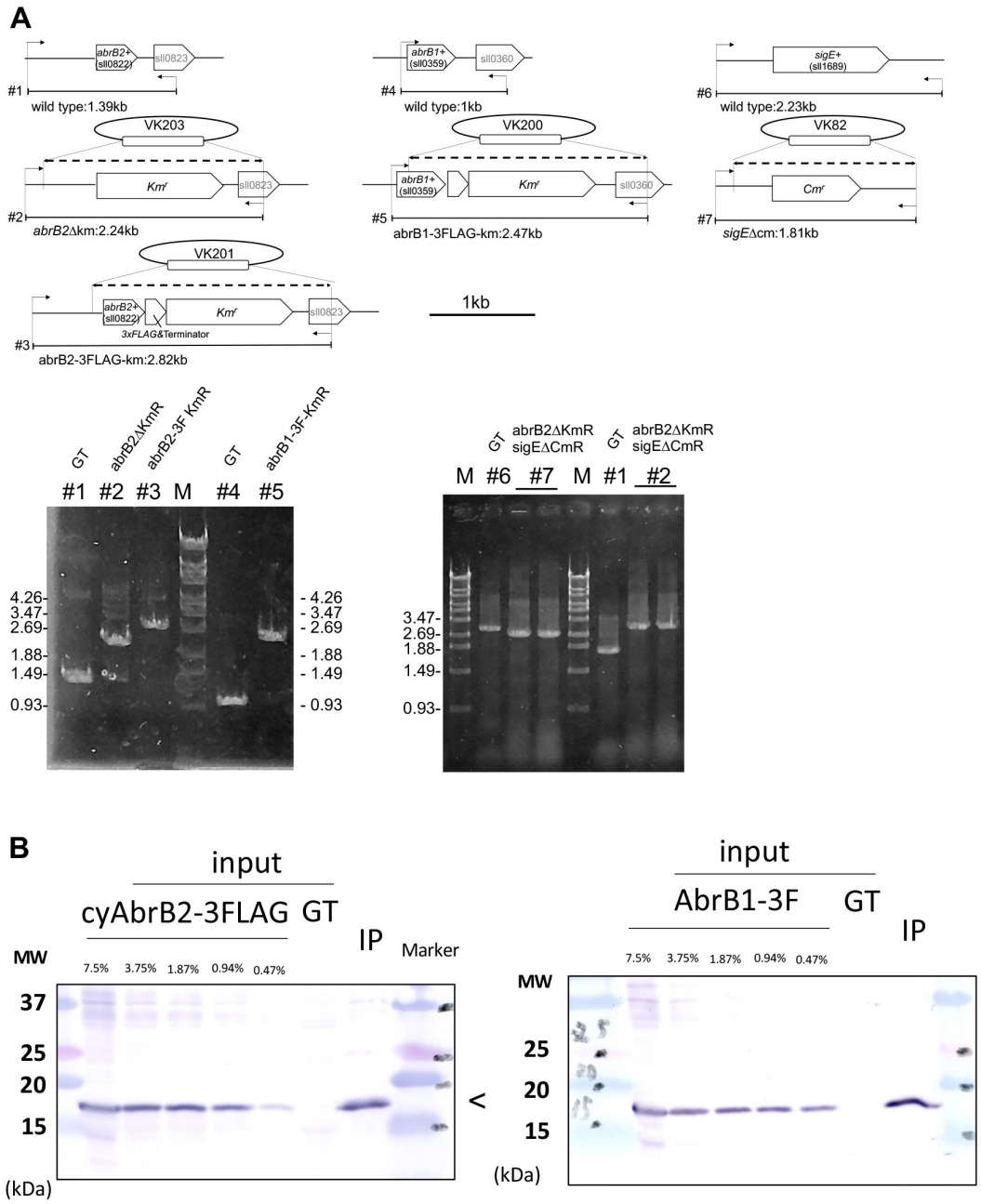

Figure S2

Genotyping and the procedure for ChIP-seq of flag-tagged proteins

Validation of procedure for ChIP-seq of flag-tagged cyAbrB2, SigE, and SigA. (A) Confirmation of genomic deletion and the epitope tagging of *abrB2* (#1-#3), the epitope tagging of *abrB1* (#4 and #5), and deletion of *sigE* (#6 and #7). Dotty lines are homologous regions between plasmids and the genome. Arrows indicate position of check primers. (B) The immunoblot for inputs and immunoprecipitants of ChIP for cyAbrB2-FLAG and cyAbrB1-FLAG. Inputs equivalent to the indicated portion of IP were loaded. (C)Scatter plots showing the reproducibility of two replicates for ChIP-seq assay. ChIP-seq data of SigE, SigA, and cyAbrB2 in aerobic and microoxic conditions and ChIP-seq data of cyAbrB1 in the aerobic condition are shown. Dots indicate normalized IP read count / normalized input read count in each 100bp window. X-axis is the value of replicate1, and Y-axis is the value of replicate 2. (D) Reproducibility of ChIP-seq data of SigA and SigE, compared with the previous study (Kariyazono and Osanai 2022). (top) Pie charts show the overlapping of peaks called in this study and the previous study. (bottom) Scatter plot comparing ChIP binding signals of SigA and SigE peaks commonly called in present and previous studies. Plots boxed by dashed lines are peaks called only in the present or previous study.

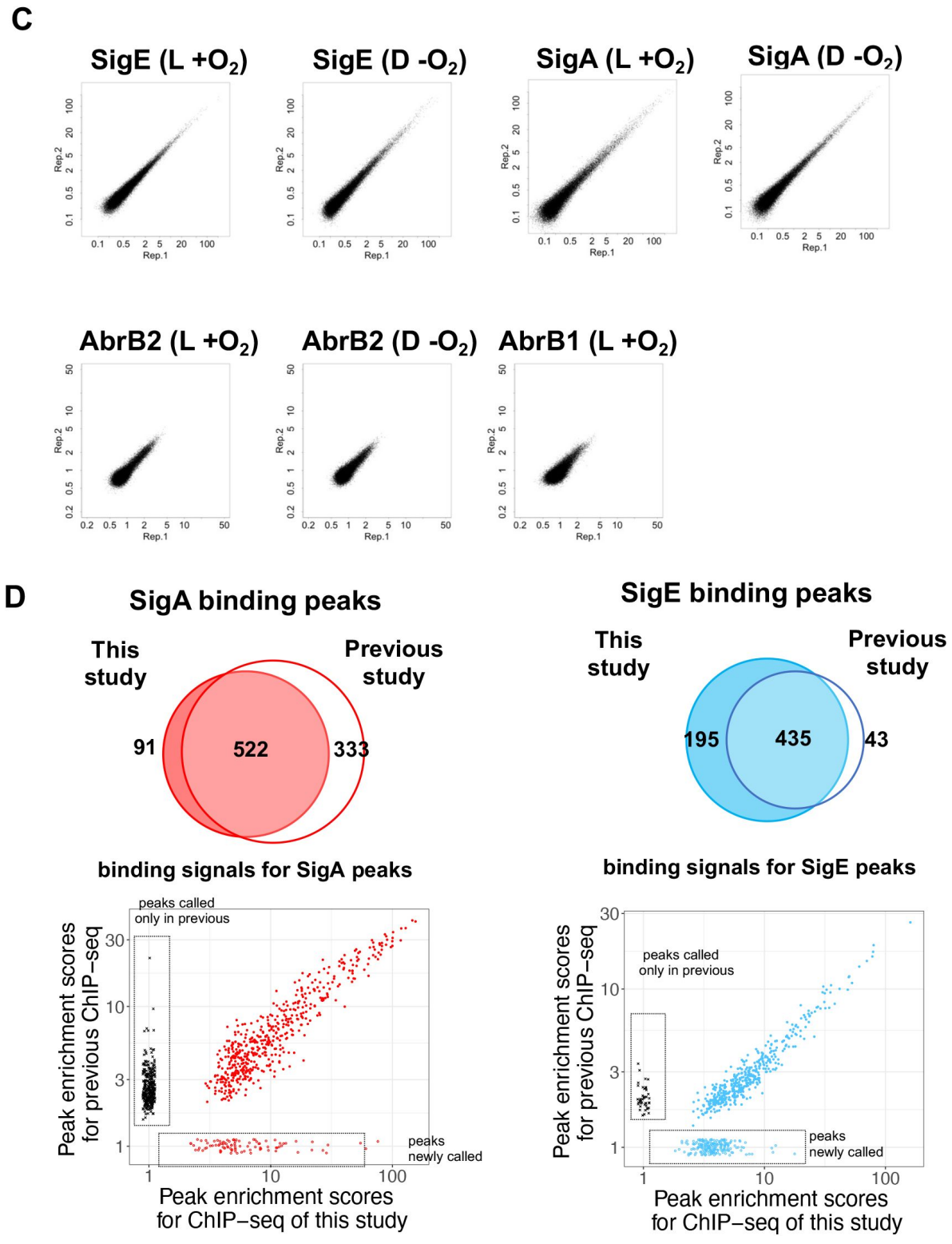

Figure S2 (continued)

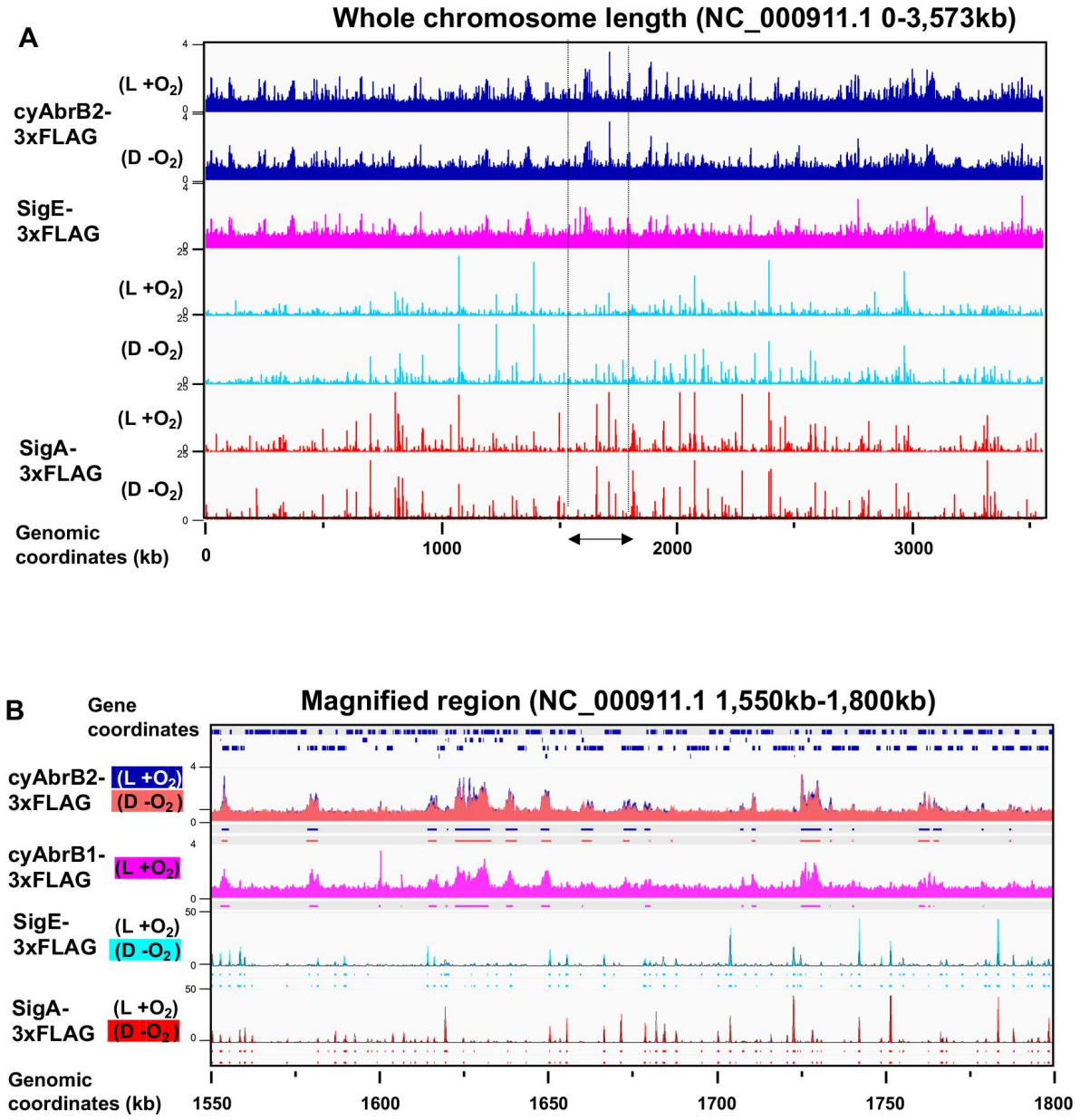

Figure S3

Overview of ChIP-seq data

Overview for ChIp-seq of flag tagged cyAbrB2, cyAbrB1, SigE, and SigA. Y-axis indicates [normalized IP read count / normalized input read count at each 25bp window], and X-axis indicates chromosome position. (A) Distribution of cyAbrB2, cyAbrB1, SigE, and SigA across the whole genome of *Synechocystis*. Aerobic (L +O2) and dark microoxic (D -O2) data are displayed. (B) Magnified image for chromosome position of 1,550kb-1,800kb. ChIP-seq data of cyAbrB2, cyAbrB1, SigE, and SigA in aerobic and dark microoxic conditions are overlayed. The dots below the graph indicate the binding region of each protein calculated by peak caller.

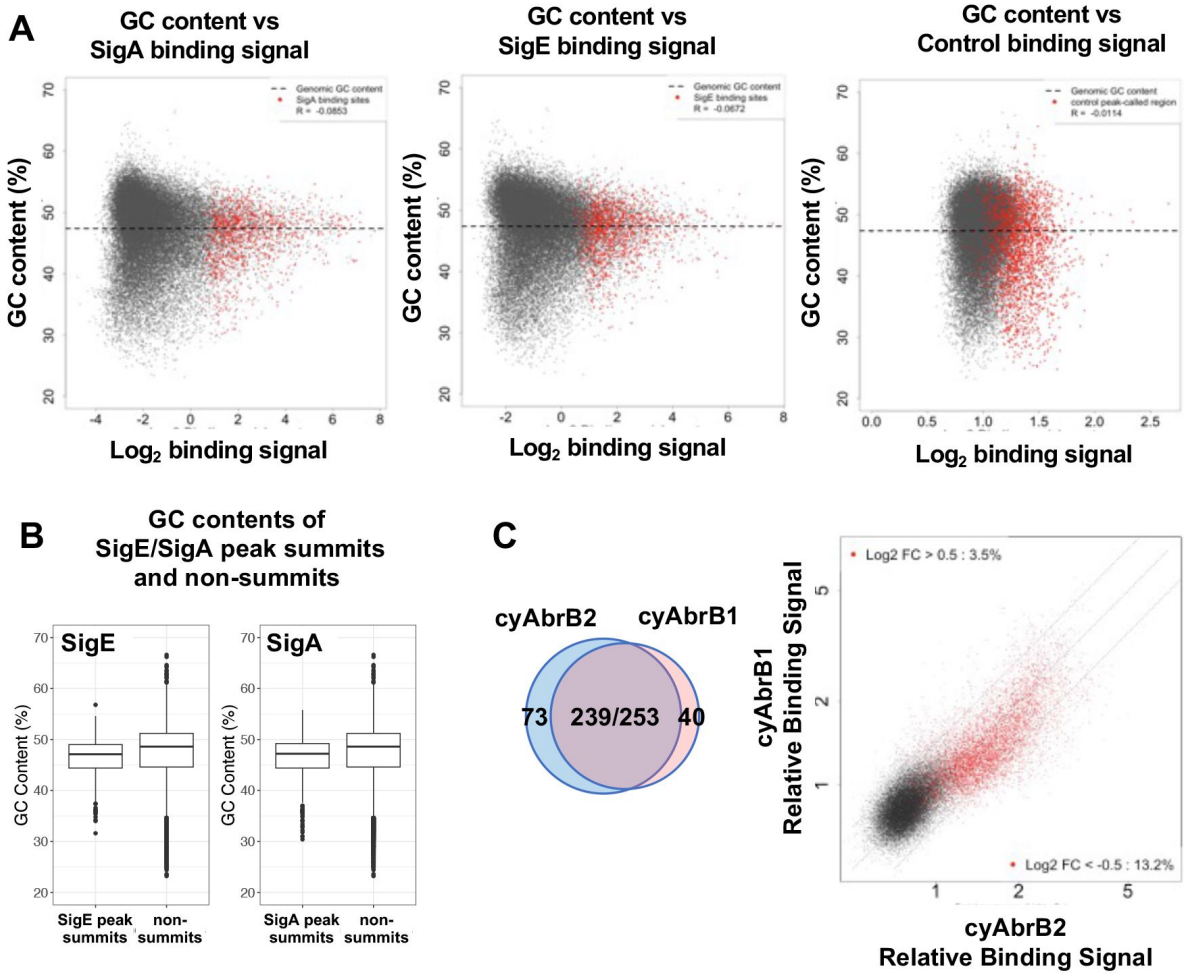

Figure S4

GC content vs ChIP enrichment score of SigA and SigE

(A) Scatter plot showing GC contents in each 100bp vs. binding signal of SigA, SigE, and control IP. Data are displayed as in **Figure 3C**. (B) GC content in each 100bp of (left) SigE peaks and non-SigE peaks, and (right) SigA peaks and non-SigA peaks. (C) Venn diagram showing overlap of the binding region of cyAbrB1 and cyAbrB2 (left), and scatter plot showing ChIP binding signal of cyAbrB2 (y-axis) and cyAbrB1(x-axis) in the aerobic condition. Data is plotted as in **Figure 4E**.

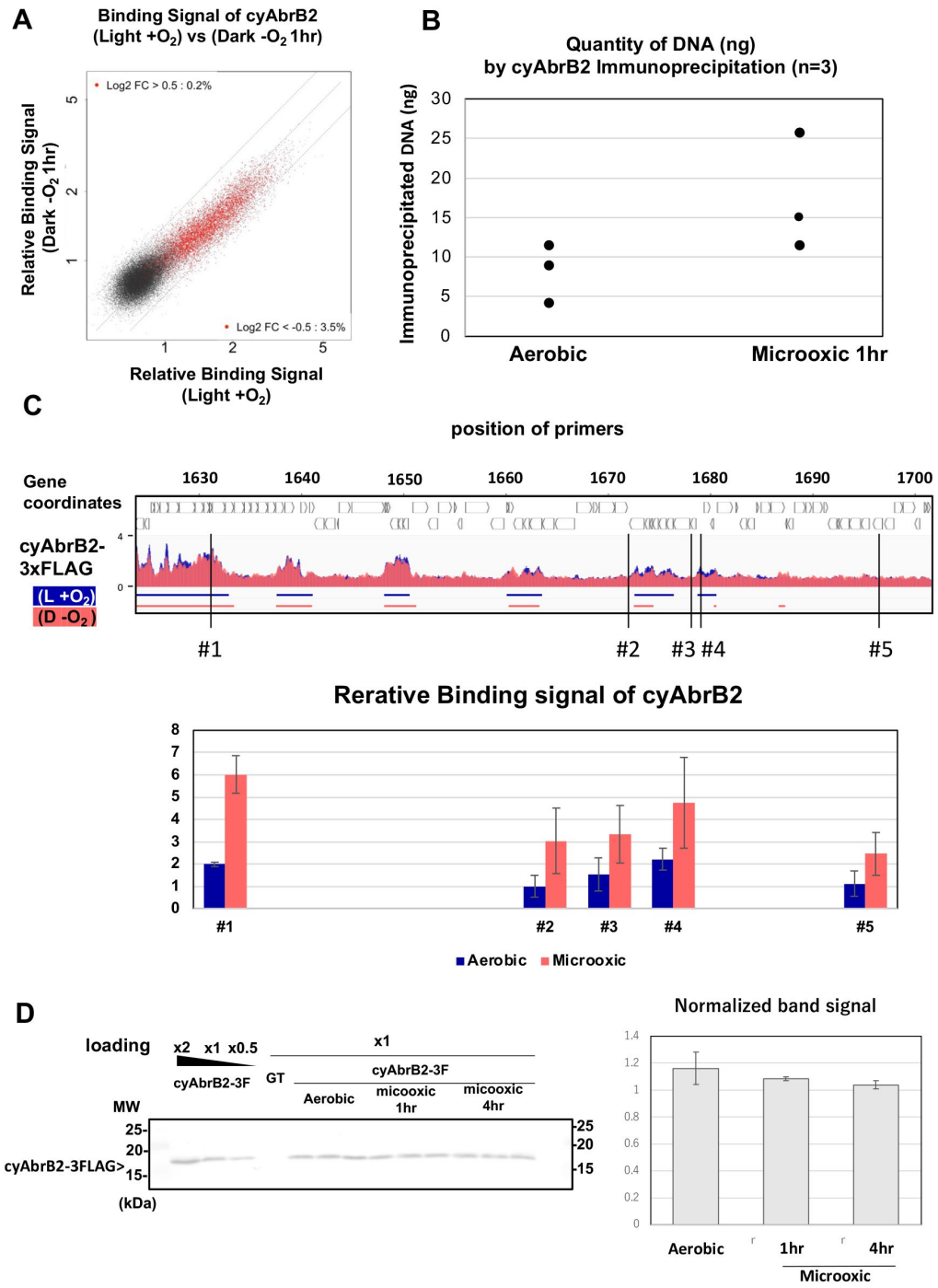

Figure S5

Alteration of cyAbrB2 binding to genome under the microoxic condition

(A) Scatter plot showing changes of the binding signal by 1hr cultivation in the microoxic condition. The binding signal of each 100bp window is plotted. Red dots are cyAbrB2 binding regions in either aerobic or microoxic conditions. The dotty lines indicate Log2 fold enrichment of 0.5, 0, -0.5 between aerobic and microoxic conditions. (B) Amount of precipitated DNA by cyAbrB2 ChIP. Three experiments were performed in the aerobic and microoxic conditions. (C) Quantification for ChIP of cyAbrB2 by qPCR. The position of primers and ChIP-seq data of cyAbrB2 are shown at the top. (D) Western blot images of cyAbrB2-3FLAG. Proteins were extracted in the aerobic condition and 1hr and 4hr incubation under microoxic conditions. The total protein concentration of each sample was adjusted to 4mg/mL, measured by the BCA method. Quantification of cyAbrB2 from western blot image was performed by ImageJ (ver. 2.0.0-rc-65) and plotted in the right graph.

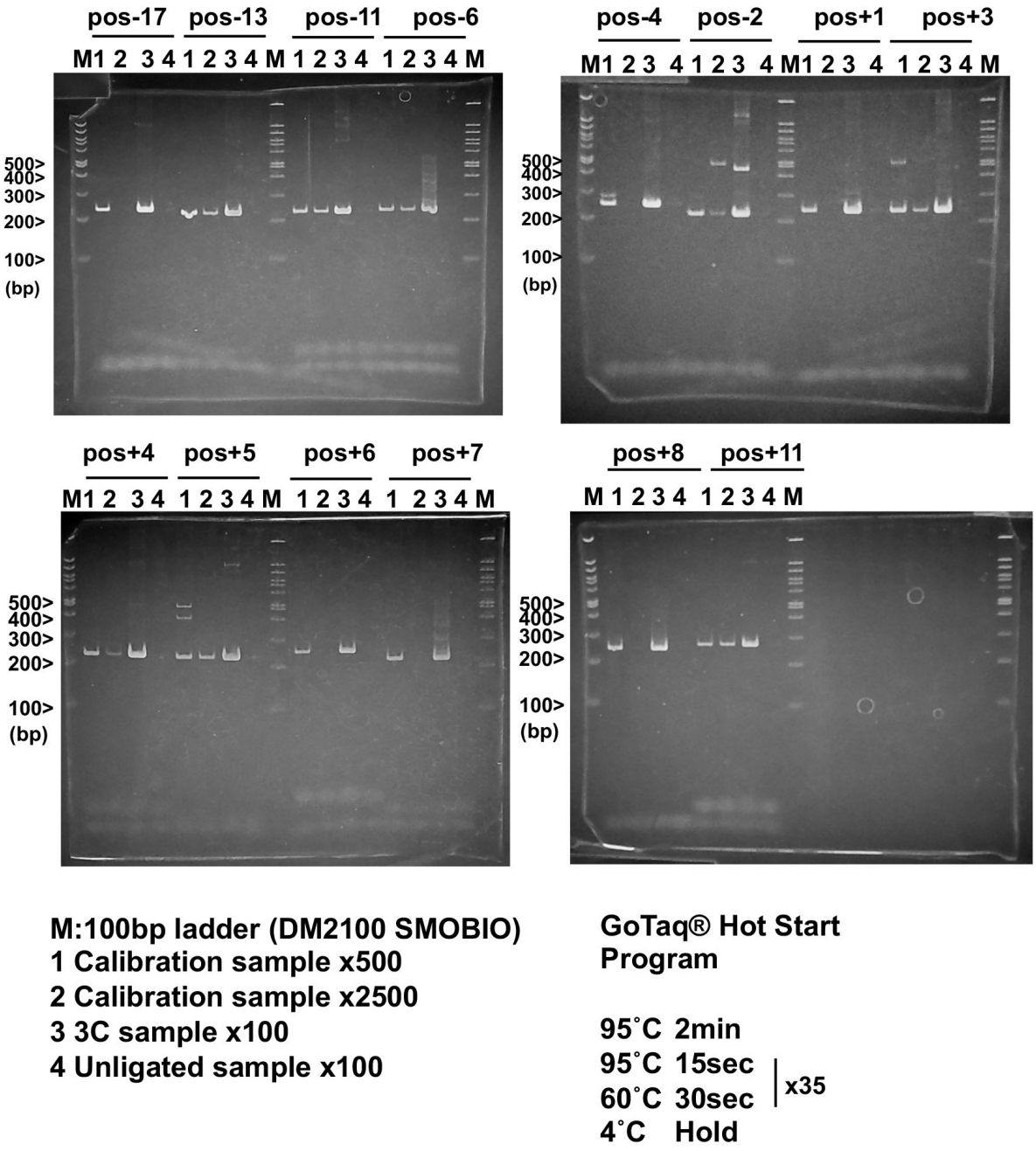

Figure S6

Validation of unidirectional primer sets for 3C assay

The validation of unidirectional primer sets for 3C assay is shown in **Figure 5**. The 3C sample in this assay is the mixture of all 3C samples assayed in **Figure 5**.

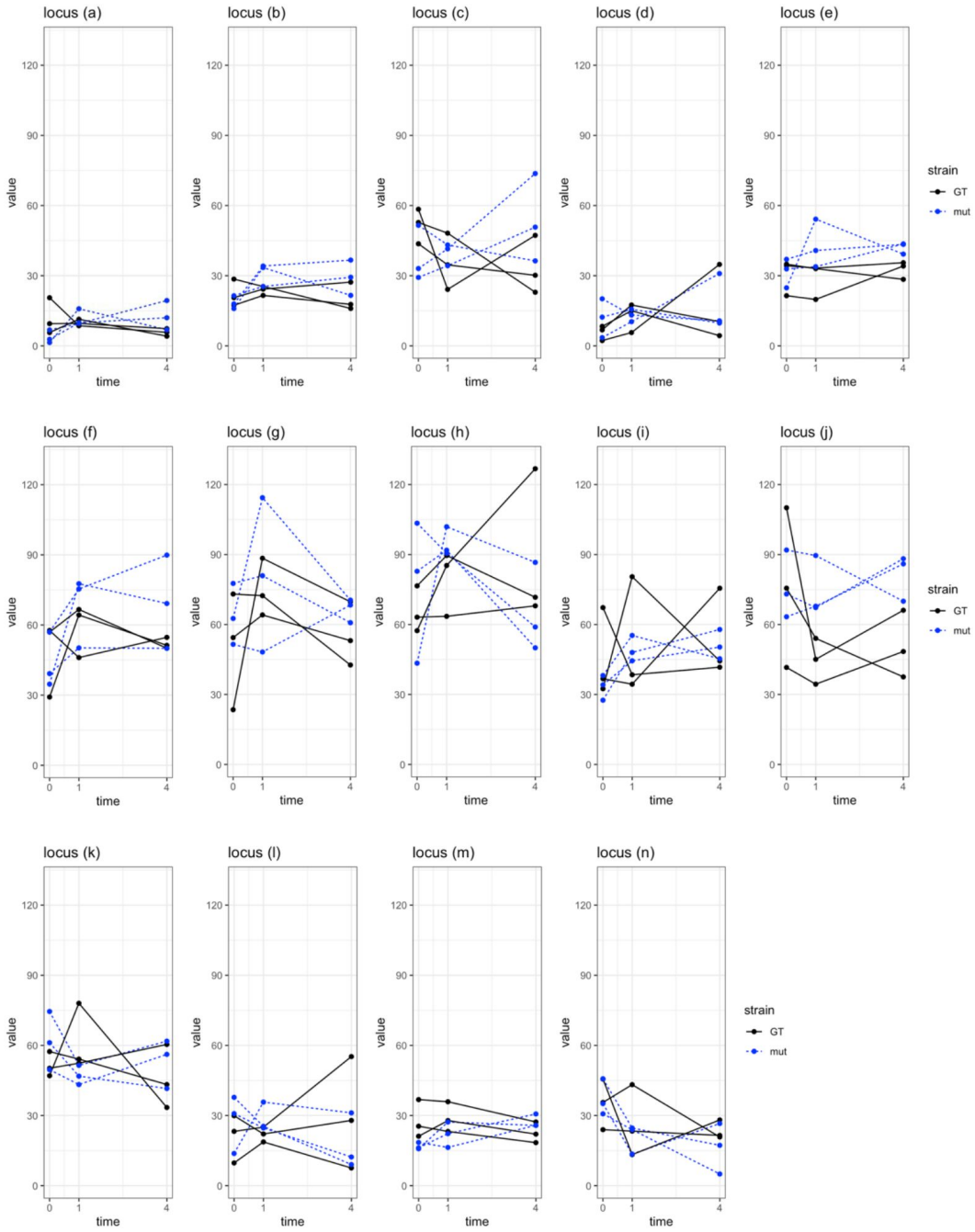

Figure S7

Dynamics of individual 3C scores

Re-plotting of **Figure 5B and 5C** with the x-axis showing time (0,1,4 hr in microoxic conditions) and the y-axis showing the interaction frequency. Plots from the individual samples are connected by solid (Wildtype) or dotty (Δ*cyabrb2*) lines.

		0hr vs 1hr		1hr vs 4hr	
Sigma factor	**locus**	**Log2FC**	**FDR**	**Log2FC**	**FDR**
SigA	slr0653	-0.873248	0.00766486	-0.0013514	0.99797563
SigB	sll0306	1.38098826	8.42E-06	0.77453605	0.04057775
SigC	sll0184	2.97101055	1.75E-16	1.30743549	0.00067892
SigD	sll2012	0.4701823	0.1498473	-0.4522181	0.32402556
SigE	sll1689	-1.9111759	1.96E-11	-1.1223298	0.00633142

Data is extracted from Supplemental Table S7.

Table S1

Fold changes of transcripts from *sigA, sigB, sigC, sigD, and sigE*

Strain ID	**Host strain**	**genotype**	**Reference**
GT			Williams, 1988
G50	GT	Δ*sigE::*KmR	T. Osanai, et al,2005
KR93	GT	SigA-8His-KmR	(Kariyazono and Osanai 2022)
KR94	GT	SigA-3FLAG-KmR	(Kariyazono and Osanai 2022)
KR340	GT	Δ*cyabrb2::*KmR	in this study
KR338	GT	cyAbrB(sll0359)-3xFLAG-KmR	in this study
KR339	GT	cyAbrB2(sll0822)-3xFLAG-KmR	in this study
KR359	KR340	Δ*cyabrB2::*KmR Δ*sigE::*CmR	in this study

Table S2

List of strains used in this study

Plasmid ID		backbone	
VK82	*sigE*ΔCmR	pTA2 (Toyobo)	transformation for KR359
VK200	AbrB1-3F-KmR	pTA2 (Toyobo)	transformation for KR338
VK201	AbrB2-3F-KmR	pTA2 (Toyobo)	transformation for KR339
VK203	*cyabrB2*ΔKmR	pTA2 (Toyobo)	transformation for KR340

Table S3

plasmids used in this study

Oligonucleotides ID		sequence
qPCR_hoxF_F	Figure S1	GTCATCTGCAATGCTGACGAA
qPCR_hoxF_R	Figure S1	CCAACACACTGCGGTCCAT
qPCR_hoxH_F	Figure S1	TCCCGTTACCCGGATTGA
qPCR_hoxH_R	Figure S1	GCCCTGGTCGTTGAGGAAA
qPCR_nifJ_sll0741_F	Figure S1	GATTCGGGGCAAAGTTTACG
qPCR_nifJ_sll0741_R	Figure S1	TACCTGGATGGTGAACTTAG
qPCR_sll0744_F	Figure S1	GCAGCTTAAATGGTTCTACC
qPCR_sll0744_R	Figure S1	CCAAATCTGTGGGTACGTAG
qPCR_nrpB_F	Figure S1	AAAGGGTAAGGGTGCAAAGG
qPCR_nrpB_R	Figure S1	AATTCCTCAAGCGGTTCCAC
new_abrB_0822_del_chkF	Figure S2A	AATCCTCCGCCAAACTTTG
abrB_0822_tag4	Figure S2A	GGAGTTTTCACCATCAGTC
abrB_0359_chkF	Figure S2A	AGAGGGAAAAATTCCTCGGC
abrB_0359_tag4	Figure S2A	TCGCCAGGGAAAGTAATTGG
SigE_whole_del_chkF	Figure S2A	GGAACGCTTGGAATGGCAAC
sigE_tag4	Figure S2A	TGAAGGGGGTAGATTTAAGCC
ChIP_slr2118_F1	Figure S5C #1	CATTTCAAGCGAGATAGCAG
ChIP_slr2118_R1	Figure S5C #2	TGGAAAGTGCCTGTTCAAAG
ChIP_ThoxH_F	Figure S5C #2	CATCACCGAGGGCATATCTAG
ChIP_ThoxH_R	Figure S5C #2	ACATAAGGCTATGGAAACC
ChIP_pHox_2F	Figure S5C #3	ACAGAGGATGGACAAATGTC
ChIP_pHox_2R	Figure S5C #3	TACCGCTTCGTCATTCTGCT
ChIP_pHox_up_2R	Figure S5C #4	TCGATTACTTCCCTTTAGTG
ChIP_pHox_up_2F	Figure S5C #4	CTTCGGCTCCATGTATTC
ChIP_sll0814_F	Figure S5C #5	GTTACTACCGCTATCTATCG

Table S4

oligonucleotides used in this study

ChIP_sll0814_R	Figure S5C #5	ATGACGTAAACCGGCTCTGAC
3Chox_Hcommon	Figure 5	CGGTCCCTTTGGACGTAATC
3Chox_H01_pos_+1	Figure 5	GGGTTGGGCGCAACATTAAG
3Chox_H02_pos_+3	Figure 5	CAAAGCGATTTTGGCTGGTG
3Chox_H03_pos_+4	Figure 5	GATGTGGTGGAAGATACGGAC
3Chox_H04_pos_+5	Figure 5	GGAGCCACAGGGGAATTTAAC
3Chox_H05_pos_+6	Figure 5	GGTCAGATTTTATTGGTTGCATGG
3Chox_H06_pos_+7	Figure 5	TTGTCAATGTCAACCGCAAC
3Chox_H07_pos_+8	Figure 5	TTATTGCCCAATCTGGCGAC
3Chox_H08_pos_+11	Figure 5	AGGCAAGACAGATAAACCTTCTG
3Chox_H09_pos_-2	Figure 5	GGGGCATAGGGAGCAAACC
3Chox_H10_pos_-4	Figure 5	GGGGTAGTACCGGAAGTGG
3Chox_H11_pos_-6	Figure 5	TTGGGCTGATTCTTGCAATTC
3Chox_H12_pos_-11	Figure 5	AGCTTTTGTCTAACACCGTATCG
3Chox_H13_pos_-13	Figure 5	AAGCCATCCTTCAAAACCCG
3Chox_H14_pos_-17	Figure 5	GCCCCATCGGTGAGAAAAAG
qPCR_hoxF_F	Figure 5 (internal control)	GTCATCTGCAATGCTGACGAA
qPCR_hoxF_R	Figure 5 (internal control)	CCAACACACTGCGGTCCAT

Table S4 (continued)

References

1. Stal L. J., Moezelaar R. (1997) **Fermentation in cyanobacteria FEMS Microbiol** *Rev* **21**:179–211

2. Osanai T., et al. (2015) **Genetic manipulation of a metabolic enzyme and a transcriptional regulator increasing succinate excretion from unicellular cyanobacterium Front** *Microbiol* **6**

3. Iijima H., et al. (2021) **Four-carbon dicarboxylic acid production through the reductive branch of the open cyanobacterial tricarboxylic acid cycle in Synechocystis sp. PCC 6803** *Metab. Eng.* **65**

4. Iijima H., et al. (2016) **Metabolomics-based analysis revealing the alteration of primary carbon metabolism by the genetic manipulation of a hydrogenase HoxH in Synechocystis sp. PCC 6803** *Algal Res.* **18**:305–313

5. Carrieri D., Wawrousek K., Eckert C., Yu J., Maness P.-C. (2011) **The role of the bidirectional hydrogenase in cyanobacteria** *Bioresour. Technol* **102**:8368–8377

6. Puggioni V., Tempel S., Latifi A. (2016) **Distribution of Hydrogenases in Cyanobacteria: A Phylum- Wide Genomic Survey** *Front. Genet* **7**

7. Cassier-Chauvat C., Veaudor T., Chauvat F. (2014) **Advances in the function and regulation of hydrogenase in the cyanobacterium Synechocystis PCC6803** *Int. J. Mol. Sci* **15**:19938–19951

8. Gutekunst K., et al. (2014) **The bidirectional NiFe-hydrogenase in Synechocystis sp. PCC 6803 is reduced by flavodoxin and ferredoxin and is essential under mixotrophic, nitrate-limiting conditions** *J. Biol. Chem.* **289**:1930–1937

9. Appel J., Phunpruch S., Steinmüller K., Schulz R. (2000) **The bidirectional hydrogenase of Synechocystis sp. PCC 6803 works as an electron valve during photosynthesis** *Arch. Microbiol.* **173**:333–338

10. Artz J. H., et al. (2020) **The structure and reactivity of the HoxEFU complex from the cyanobacterium Synechocystis sp. PCC 6803** *J. Biol. Chem* **295**:9445–9454

11. Wang Y., et al. (2022) **Pyruvate:ferredoxin oxidoreductase and low abundant ferredoxins support aerobic photomixotrophic growth in cyanobacteria** *Elife* **11**

12. Burgstaller H., et al. (2022) **Synechocystis sp. PCC 6803 Requires the Bidirectional Hydrogenase to Metabolize Glucose and Arginine Under Oxic Conditions** *Front. Microbiol* **13**

13. Hołówka J., Zakrzewska-Czerwińska J. (2020) **Nucleoid Associated Proteins: The Small Organizers That Help to Cope With Stress** *Front. Microbiol* **11**

14. Behle,, et al. (2022) **Manipulation of topoisomerase expression inhibits cell division but not growth and reveals a distinctive promoter structure in Synechocystis** *Nucleic Acids Res* **50**:12790–12808

15. Summerfield T. C., Nagarajan S., Sherman L. A. (2011) **Gene expression under low-oxygen conditions in the cyanobacterium Synechocystis sp. PCC 6803 demonstrates Hik31-dependent and - independent responses** *Microbiology* **157**:301–312

16. Osanai T., et al. (2005) **Positive regulation of sugar catabolic pathways in the cyanobacterium Synechocystis sp. PCC 6803 by the group 2 sigma factor sigE** *J. Biol. Chem.* **280**:30653–30659

17. Osanai T., et al. (2011) **Genetic engineering of group 2 sigma factor SigE widely activates expressions of sugar catabolic genes in Synechocystis species PCC 6803** *J. Biol. Chem* **286**:30962–30971

18. Dutheil J., et al. (2012) **The AbrB2 autorepressor, expressed from an atypical promoter, represses the hydrogenase operon to regulate hydrogen production in Synechocystis strain PCC6803** *J. Bacteriol* **194**:5423–5433

19. Leplat,, et al. (2013) **Genome-wide transcriptome analysis of hydrogen production in the cyanobacterium Synechocystis: Towards the identification of new players** *Int. J. Hydrogen Energy* **38**:1866–1872

20. Oliveira P., Lindblad P. (2008) **An AbrB-Like protein regulates the expression of the bidirectional hydrogenase in Synechocystis sp. strain PCC 6803** *J. Bacteriol* **190**:1011–1019

21. Gutekunst K., et al. (2005) **LexA regulates the bidirectional hydrogenase in the cyanobacterium Synechocystis sp. PCC 6803 as a transcription activator** *Mol. Microbiol* **58**:810–823

22. Oliveira P., Lindblad P. (2005) **LexA, a transcription regulator binding in the promoter region of the bidirectional hydrogenase in the cyanobacterium Synechocystis sp. PCC 6803** *FEMS Microbiol. Lett.* **251**:59–66

23. Imamura S., Asayama M. (2009) **Sigma factors for cyanobacterial transcription** *Gene Regul. Syst. Bio* **3**:65–87

24. Kariyazono R., Osanai T. (2022) **Identification of the genome-wide distribution of cyanobacterial group- 2 sigma factor SigE, accountable for its regulon** *Plant J* **110**:548–561

25. Higo, E. Nishiyama, K. Nakamura, Y. Hihara, S. Ehira (2019) **cyAbrB Transcriptional Regulators as Safety Devices To Inhibit Heterocyst Differentiation in Anabaena sp. Strain PCC 7120** *J. Bacteriol* **201**

26. Ishii, Y. Hihara (2008) **An AbrB-like transcriptional regulator, Sll0822, is essential for the activation of nitrogen-regulated genes in Synechocystis sp. PCC 6803** *Plant Physiol.* **148**:660–670

27. Lieman-Hurwitz J., et al. (2009) **A cyanobacterial AbrB-like protein affects the apparent photosynthetic affinity for CO2 by modulating low-CO2-induced gene expression** *Environ. Microbiol* **11**:927–936

28. Yamauchi Y., Kaniya Y., Kaneko Y., Hihara Y. (2011) **Physiological roles of the cyAbrB transcriptional regulator pair Sll0822 and Sll0359 in Synechocystis sp. strain PCC 6803** *J. Bacteriol* **193**:3702–3709

29. Uyeda K., Rabinowitz J. C. (1971) **Pyruvate-ferredoxin oxidoreductase. 3. Purification and properties of the enzyme** *J. Biol. Chem* **246**:3111–3119

30. Vignais P. M., Billoud B. (2007) **Occurrence, classification, and biological function of hydrogenases: an overview** *Chem. Rev* **107**:4206–4272

31. Ortega-Ramos M., et al. (2014) **Engineering Synechocystis PCC6803 for hydrogen production: influence on the tolerance to oxidative and sugar stresses** *PLoS One* **9**

32. Katayama N., Iwazumi K., Suzuki H., Osanai T., Ito S. (2022) **Malic Enzyme, not Malate Dehydrogenase, Mainly Oxidizes Malate That Originates from the Tricarboxylic Acid Cycle in Cyanobacteria** *MBio* **13**

33. Hasunuma T., Matsuda M., Kondo A. (2016) **Improved sugar-free succinate production by Synechocystis sp. PCC 6803 following identification of the limiting steps in glycogen catabolism** *Metab. Eng. Commun.* **3**:130–141

34. Song K., et al. (2022) **Expression of the Cyanobacterial F(o)F(1) ATP Synthase Regulator AtpΘ Depends on Small DNA-Binding Proteins and Differential mRNA Stability** *Microbiol. Spectr* **10**

35. Camsund T., Heidorn P., Lindblad (2014) **Design and analysis of LacI-repressed promoters and DNA-looping in a cyanobacterium** *J. Biol. Eng* **8**

36. Osanai T., et al. (2009) **ChlH, the H subunit of the Mg-chelatase, is an anti-sigma factor for SigE in Synechocystis sp. PCC 6803** *Proc. Natl. Acad. Sci. U. S. A.* **106**:6860–6865

37. Iijima H., et al. (2015) **Changes in primary metabolism under light and dark conditions in response to overproduction of a response regulator RpaA in the unicellular cyanobacterium Synechocystis sp. PCC 6803** *Front. Microbiol.* **6**

38. Williams J. G. K. (1988) **"Construction of Specific Mutations in Photosystem II Photosynthetic Reaction Center by Genetic Engineering Methods in Synechocystis 6803"** *Methods in Enzymology* :766–778

39. Rippka R., Deruelles J., Waterbury J. B. (1979) **Generic assignments, strain histories and properties of pure cultures of cyanobacteria** *J. Gen. Microbiol* **111**:1–61

40. Chen S., Zhou Y., Chen Y. (2018) **Gu, fastp: an ultra-fast all-in-one FASTQ preprocessor** *Bioinformatics* **34**:i884–i890

41. Langmead, S. L. Salzberg (2012) **Fast gapped-read alignment with Bowtie 2** *Nat. Methods* **9**:357–359

42. Anders S., Pyl P. T., Huber W. (2015) **HTSeq--a Python framework to work with high-throughput sequencing data** *Bioinformatics* **31**:166–169

43. Robinson M. D., McCarthy D. J., Smyth G. K. (2010) **edgeR: a Bioconductor package for differential expression analysis of digital gene expression data** *Bioinformatics* **26**:139–140

44. Zhang Y., et al. (2008) **Model-based analysis of ChIP-Seq (MACS)** *Genome Biol* **9**

45. Kopf M., et al. (2014) **Comparative genome analysis of the closely related Synechocystis strains PCC 6714 and PCC 6803** *DNA Res* **21**:255–266

46. Quinlan R., Hall I. M. (2010) **BEDTools: a flexible suite of utilities for comparing genomic features** *Bioinformatics* **26**:841–842

47. Shen W., Le S., Li Y., Hu F. (2016) **SeqKit: A Cross-Platform and Ultrafast Toolkit for FASTA/Q File Manipulation** *PLoS One* **11**

48. Takemata N., Samson R. Y., Bell S. D. (2019) **Physical and Functional Compartmentalization of Archaeal Chromosomes** *Cell* **179**:165–179

49. Takemata N., Bell S. D. (2021) **Chromosome conformation capture assay combined with biotin enrichment for hyperthermophilic archaea** *STAR Protoc* **2**

50. M. Abou El Hassan, R. Bremner (2009) **A rapid simple approach to quantify chromosome conformation capture** *Nucleic Acids Res* **37**

51. (2022) **R: A Language and Environment for Statistical Computing**

52. Hervé M. (2022) **RVAideMemoire: Testing and Plotting Procedures for Biostatistics**

53. Wu T., et al. (2021) **clusterProfiler 4.0: A universal enrichment tool for interpreting omics data** *Innov. (Cambridge* **2**

Article and author information

Ryo Kariyazono
School of Agriculture, Meiji University
ORCID iD: 0000-0002-7591-3117

Takashi Osanai
School of Agriculture, Meiji University
For correspondence: tosanai@meiji.ac.jp
ORCID iD: 0000-0003-2229-6028

Copyright

© 2024, Ryo Kariyazono & Takashi Osanai

This article is distributed under the terms of the Creative Commons Attribution License, which permits unrestricted use and redistribution provided that the original author and source are credited.

Editors

Reviewing Editor
Yamini Dalal
National Cancer Institute, Bethesda, United States of America

Senior Editor
Yamini Dalal
National Cancer Institute, Bethesda, United States of America

Reviewer #1 (Public Review):

Strength:
At first glance, I had a very positive impression of the overall manuscript. The experiments were well done, the data presentation looks very structured, and the text reads well in principle.

Weakness:
Having a closer look, the red line of the manuscript is somewhat blurry. Reading the abstract, the introduction, and parts of the discussion, it is not really clear what the authors exactly aim to target. Is it the regulation of fermentation in cyanobacteria because it is under-investigated? Is it to bring light to the transcriptional regulation of hydrogenase genes? The regulation by SigE? Or is it to get insight into the real function of cyAbrB2 in cyanobacteria? All of this would be good of course. But it appears that the authors try to integrate all these aspects, which in the end is a little bit counterintuitive and in some places even confusing. From my point of view, the major story is a functional investigation of the presumable transcriptional regulator cyAbrB2, which turned out to be a potential NAP. To demonstrate/prove this, the hox genes have been chosen as an example due to the fact that a regulatory role of cyAbrB2 has already been described. In my eyes, it would be good to restructure or streamline the introduction according to this major outcome.

Points to consider:
The authors suggest that the microoxic condition is the reason for the downregulation of e.g. photosynthesis (l.112-114). But of course, they also switched off the light to achieve a microoxic environment, which presumably is the trigger signal for photosynthesis-related genes. I suggest avoiding making causal conclusions exclusively related to oxygen and recommend rephrasing (for example, "were downregulated under the conditions applied").

The authors hypothesized that cyAbrB2 modulates chromosomal conformation and conducted a 3C analysis. But if I read the data in Figure 5B & C correctly, there is a lot of interaction in a range of 1650 and 1700 kb, not only at marked positions c and j. Positions c and j have been picked because it appears that cyAbrB2 deletion impacts this particular interaction. But is it really significant? In the case of position j the variation between the replicates seems quite high, in the case of position c the mean difference is not that high. Moreover, does all this correlate with cyAbrB2 binding, i.e. with positions of gray bars in panel A? If this was the case, the data obtained for the cyabrB2 mutant should look totally different but they are quite similar to WT. That's why the sentence "By contrast, the interaction frequency in Δcyabrb2 mutant were low and unchanged in the aerobic and microoxic conditions" does not fit to the data shown. But I have to mention that I am not an expert in these kinds of assays. Nevertheless, if there is a biological function that shall be revealed by an experiment, the data must be crystal clear on that. At least the descriptions of the 3C data and the corresponding conclusions need to be improved. For me, it is hard to follow the authors' thoughts in this context.

The figures are nicely prepared, albeit quite complex and in some cases not really supportive of the understanding of the results description. Moreover, they show a rather loose organization that sometimes does not fit the red line of the results section. For example, Figure 1D is not mentioned in the paragraph that refers to several other panels of the same figure (see lines110-128). Panel 1D is mentioned later in the discussion. Does 1D really fit into Figure 1 then? Are all the panels indeed required to be shown in the main document? As some elements are only briefly mentioned, the authors might also consider moving some into the supplement (e.g. left part of Figure 1C, Figure 2A, Figure 3B ...) or at least try to distribute some panels into more figures. This would reduce complexity and increase comprehensibility for future readers. Also, Figure 3 is a way too complex. Panel G could be an alone-standing figure. The latter would also allow for an increase in font sizes or to show ChIP data of both

conditions (L+O2 and D-O2) separately. Moreover, a figure legend typically introduces the content as a whole by one phrase but here only the different panels are described, which fits to the impression that all the different panels are not well connected. Of course, it is the decision of the authors what to present and how but may they consider restructuring and simplifying.

The authors assume a physiological significance of transient upregulation of e.g. hox genes under microoxic conditions. But does the hydrogenase indeed produce hydrogen under the conditions investigated and is this even required? Moreover, the authors use the term "fermentative gene". But is hydrogen indeed a fermentation product, i.e. are protons the terminal electron acceptor to achieve catabolic electron balance? Then huge amounts of hydrogen should be released. Comment should be made on this.

The authors also mention a reverse TCA cycle. But is its existence an assumption or indeed active in cyanobacteria, i.e. is it experimentally proven? The authors are a little bit vague in this regard (see lines 241-246).

https://doi.org/10.7554/eLife.94245.1.sa1

Reviewer #2 (Public Review):

This work probes the control of the hox operon in the cyanobacterium Synechocystis, where this operon directs the synthesis of a bidirectional hydrogenase that functions to produce hydrogen. In assessing the control of the hox system, the authors focused on the relative contributions of cyAbrB2, alongside SigE (and to a lesser extent, SigA and cyAbrB1) under both aerobic and microoxic conditions. In mapping the binding sites of these different proteins, they discovered that cyAbrB2 bound many sites throughout the chromosome repressed many of its target genes, and preferentially bound regions that were (relatively) rich in AT-residues. These characteristics led the authors to consider that cyAbrB2 may function as a nucleoid-associated protein (NAP) in Synechocystis, given its functional similarities with other NAPs like H-NS. They assessed the local chromosome conformation in both wild-type and cyabrB2 mutant strains at multiple sites within a 40 kb window on either side of the hox locus, using a region within the hox operon as bait. They concluded that cyAbrB2 functions as a nucleoid-associated protein that influences the activity of SigE through its modulation of chromosome architecture.

The authors approached their experiments carefully, and the data were generally very clearly presented and described.

Based on the data presented, the authors make a strong case for cyAbrB2 as a nucleoid-associated protein, given the multiple ways in which it seems to function similarly to the well-studied Escherichia coli H-NS protein. It would be helpful to provide some additional commentary within the discussion around the similarities and differences of cyAbrB2 to other nucleoid-associated proteins, and possible mechanisms of cyAbrB2 control (post-translational modification; protein-protein interactions; etc.). The manuscript would also be strengthened with the inclusion of biochemical experiments probing the binding of cyAbrB2, particularly focussing on its oligomerization and DNA polymerization/bridging potential.

Previous work had revealed a role for SigE in the control of hox cluster expression, which nicely justified its inclusion (and focus) in this study. However, the results of the SigA studies here suggested that SigA both strongly associated with the hox promoter, and its binding sites were shared more frequently than SigE with cyAbrB2. The focus on cyAbrB2 is also well-justified, given previous reports of its control of hox expression; however, it shares binding sites with an essential homologue cyAbrB1. Interestingly, while the B1 protein appears to bind similar sites, instead of repressing hox expression, it is known as an activator of this

operon. It seems important to consider how cyAbrB1 activity might influence the results described here.

https://doi.org/10.7554/eLife.94245.1.sa0